REPORT DOCUMENTATION PAGE

Form Approved
OMB No. 0704-0188

1. AGENCY USE ONLY (Leave blank)	2. REPORT DATE	3. REPORT TYPE AND DATES COVERED
	17 Oct 90	technical

4. TITLE AND SUBTITLE
Signal Processing Studies of a Simulated Laser Doppler Velocimetry-Based Acoustic Sensor
Technical Report under Contract N00014-89-J-1967

5. FUNDING NUMBERS
N00014-89-J-1967

6. AUTHOR(S)
Barlett, Martin L.

7. PERFORMING ORGANIZATION NAMES(S) AND ADDRESS(ES)
Applied Research Laboratories
The University of Texas at Austin
P.O. Box 8029
Austin, Texas 78713-8029

8. PERFORMING ORGANIZATION REPORT NUMBER
ARL-TR-90-33

9. SPONSORING/MONITORING AGENCY NAME(S) AND ADDRESS(ES)
Office of the Chief of Naval Research
Department of the Navy
Arlington, Virginia 22217-5000

10. SPONSORING/MONITORING AGENCY REPORT NUMBER

11. SUPPLEMENTARY NOTES

12a. DISTRIBUTION/AVAILABILITY STATEMENT
Approved for public release; distribution is unlimited.

12b. DISTRIBUTION CODE

13. ABSTRACT (Maximum 200 words)

In this report we discuss a possible remote acoustic sensing scheme based on laser Doppler velocimetry (LDV). The signal characteristics of an LDV signal from single particle scattering are described for differential and reference beam LDV configurations. A model is developed to simulate LDV signals which includes shot noise and random phase and additive noise contributions. Comparisons are made between results obtained from simulated and actual LDV signals using several signal processing techniques. The effects of various noise sources on LDV signal detectability and sensitivities to various optical parameters are studied using power spectral methods and a simulated LDV signal. Enhanced signal detectability in random noise backgrounds is investigated using spectral correlation methods. Results indicate that it may be possible to extend demonstrated LDV-based acoustic sensor sensitivities using higher order processing techniques.

14. SUBJECT TERMS

remote acoustic sensing	laser Doppler velocimetry (LDV)	LDV signal simulation	
backscatter LDV configurations	LDV noise studies	power spectral processing	
spectral correlation processing	co-intensity	scattered flux calculations	

15. NUMBER OF PAGES
64

16. PRICE CODE

17. SECURITY CLASSIFICATION OF REPORT	18. SECURITY CLASSIFICATION OF THIS PAGE	19. SECURITY CLASSIFICATION OF ABSTRACT	20. LIMITATION OF ABSTRACT
UNCLASSIFIED	UNCLASSIFIED	UNCLASSIFIED	SAR

TABLE OF CONTENTS

LIST OF FIGURES

EXECUTIVE SUMMARY

In this report we have described efforts to understand the principles of laser Doppler velocimetry (LDV) based remote acoustic detection, the general characteristics of signals produced by LDV sensors, factors which limit the sensitivity of such systems, and the relative merits of several different processing schemes for LDV acoustic sensors. The basic single particle forms of LDV signals for two optical arrangements, the differential and reference beam geometries, have been derived and used as the basis for constructing an LDV signal simulation program for use in signal processing studies. The simulated signals consist of a "photon stream" which represents the output from a photon-counting detector. The noise contribution due to the discrete nature of the detection process (shot noise) is simulated using a Poisson distributed random number generator. Additional terms are incorporated in the signal which allow the user to specify the relative contributions of random phase noise and additive random noise to the signal.

In constructing a simulation model for an LDV signal we have attempted to include the signal properties which are most relevant from a signal processing perspective. Comparisons of results obtained from several different signal processing algorithms using both simulated LDV signals and a sample of actual LDV data suggest that the simulated signals are a reasonable representation of signals which may be obtained from an actual LDV acoustic sensor. The signal simulation program was used extensively in the signal processing studies which followed. This program provided a great deal of flexibility in specifying the signal characteristics (Doppler signal strength, signal-to-noise ratios, detected photon flux, etc.) for determination of the merits and limitations of various signal processing schemes.

The initial signal processing study utilized power spectral processing to identify the effects of the model noise sources on the detectability of the Doppler signal. The relationship between the Doppler signal strength and the underlying acoustic field was established. Also general relationships were determined which related the maximum tolerable noise levels from the various sources to the minimum Doppler signal which could be visually identified in a power spectral plot. Several limitations on Doppler signal detectability were

empirically determined during the course of the study. Lower limits were established for the detected photon flux as a function of Doppler signal strength for a "noiseless" LDV acoustic sensor. The effects of the various model noise sources were then investigated and maximum noise levels as a function of Doppler signal strength were determined. Based on the empirical results of this study, one can conclude that an extension of demonstrated detection sensitivity by one or two orders of magnitude will require a very "quiet" LDV system if power spectral processing techniques are employed.

Motivated by the relationship between signal detectability and detected photon flux, a set of calculations was then performed to determine the viability of detecting weak acoustic fields in a laboratory demonstration using LDV techniques. The scattered photon flux at a photodetector was determined for two possible LDV configurations constrained to operate in a backscatter geometry. The sensitivity to the various optical parameters of the LDV system was also determined. Uncertainties about both the value and applicability of the seawater scattering coefficient used in the calculations raised concerns about the validity of the results. However, based on the inputs used in the calculations, a laboratory demonstration of LDV acoustic sensing appears feasible at sound levels which are one or two orders of magnitude less than those presently detected in laboratory measurements. The uncertainties in the seawater scattering characteristics are being addressed in a separate experimental program.

Finally, an initial study was conducted of several potential higher order processing techniques which may provide better discrimination against certain noise sources than can be obtained from power spectral techniques. The methods used in this study employ spectral correlation techniques which highlight fixed phase relationships between various spectral components. Bispectral techniques were not evaluated due to the limitations of the signal forms which can presently be simulated; evaluation of bispectral processing schemes has been left for a future study.

An empirical evaluation of a standard spectral correlation function known as the co-intensity was performed and compared with results from power spectral analysis. The comparisons indicated enhanced processing gain in the

presence of random noise sources using co-intensity processing; the comparison also suggested that detection of the Doppler signal may be possible in random noise backgrounds with levels which are approximately twice as large as the maximum tolerable noise levels found in the power spectral processing studies. A more detailed determination of the limitations of this technique remains for a future study. A new algorithm, which utilizes spectral correlation techniques and attempts to exploit symmetries which exist in the LDV spectrum, was developed. Comparisons of results from this "folded co-intensity" with conventional co-intensity results suggest that the folded co-intensity technique may provide enhanced detection coherence for this form of signal.

1. INTRODUCTION

This report describes a technique known as laser Doppler velocimetry (LDV), which may potentially provide a means for remotely sensing acoustic fields in a fluid. This report also discusses the basic principles of LDV measurements and describes the fundamental characteristics of signals generated from LDV systems. A computer model is outlined which has been developed for simulating LDV signals based on these signal features. Based on results obtained using the signal simulation program, results are then given from a study of Doppler signal detection in the presence of noise and descriptions provided for some of the limitations on signal detectability which various noise sources may produce. The effects of various optical arrangements on laboratory LDV measurements of an acoustic field are calculated and the merits and limitations of various optical configurations are identified. Finally, a study of several higher order processing methods is reported and comparisons are made between results obtained from conventional power spectral techniques and from potential higher order processing schemes. The results of these investigations indicate that higher order processing methods may achieve better sensitivities in noise limited LDV systems.

The possibility of extending LDV acoustic sensor sensitivity has important implications for naval applications. Due to the virtual nature of this form of sensor which employs beams of coherent light as sensors, the potential exists for developing acoustic sensor arrays of arbitrary configurations (vertical arrays, spherical arrays, etc.) which may be readily "deployed" from a moving platform. However, the sensitivity to acoustic fields attainable using present LDV systems and present signal processing methods are not sufficient to be of tactical use in naval applications. The possibility of extending the sensitivity of these systems, primarily through improved signal processing techniques, serves as the motivation for the work reported here.

2. SIGNAL CHARACTERISTICS OF LASER DOPPLER VELOCIMETRY SYSTEMS

There have been a number of experiments to demonstrate the detection of an acoustic field using various laser-based optical configurations as remote acoustic sensors.[1-8] Although the details of these systems vary greatly, they can be classified into three broad categories (1) homodyne and (2) heterodyne detection systems and (3) Schlieren systems. The first two methods rely on detection of a Doppler shift in the scattered light, while the Schlieren method utilizes spatial variations of the detected light caused by perturbations of the refractive index of the acoustic medium as an acoustic wave propagates. Heterodyne detection is by far the most popular technique and is generally believed to be the method best suited for remote acoustic sensing in an underwater environment.

The "signal" in an LDV system arises from scattering of the illuminating laser light from a moving scattering center. For a moving scatterer, the change in frequency of the scattered light (Doppler shift) is given by

$$\Delta f = \frac{2v}{\lambda} \cos\beta \sin\frac{\alpha}{2} \quad , \tag{2.1}$$

where

- $v \cos\beta$ is the magnitude of the scattering center velocity parallel to the bisector of the angle between the incident and scattered rays,
- λ is the wavelength of the illuminating radiation, and
- α is the scattering angle (see Fig. 2.1).

As can be seen from the above expression, direct spectroscopic determination of the frequency shift is possible only for relatively high velocities such as those encountered in supersonic flow. Thus it has become a standard practice to determine the Doppler shift as a frequency difference between two light beams.

In the following section, two different optical heterodyne arrangements, known generically as the dual-beam or differential configuration and the

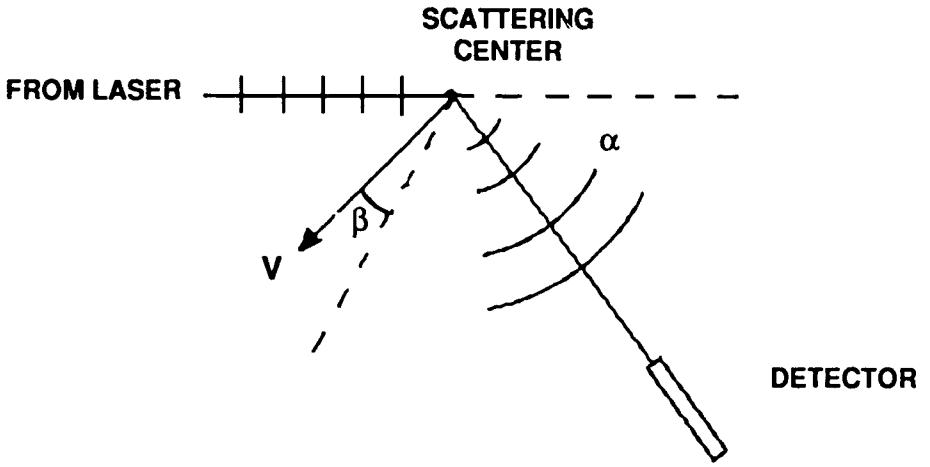

FIGURE 2.1
THE DOPPLER SHIFT IN SCATTERING
THE DOPPLER SHIFT RESULTS FROM LIGHT SCATTERING FROM A MOVING SCATTERER

reference beam arrangement, will be considered. A schematic representation of the key optical features of each configuration is shown in Fig. 2.2.

2.1 SINGLE PARTICLE SCATTERING

In order to study the signal obtained from these optical configurations, it is necessary to examine the scattering process from which the Doppler shift originates. Following the discussion of Adrian,[9] we write the electric field of the scattered light wave produced by the lth illuminating beam scattering from the jth particle as

$$E'_{lj} = \sqrt{I_l}\,\frac{\sigma_{lj}}{k|\vec{r}|}\,e^{i\phi_{lj}} \quad . \tag{2.2}$$

Here the prime denotes the scattered wave, I_l is the intensity of the illuminating beam l, k is the illuminating beam wave number ($2\pi/\lambda$), $\vec{r}$ is the vector between the illuminated particle and the observer, and σ_{lj} is the scattering coefficient for the jth particle which specifies the intensity, polarization, and phase shift of the scattered wave with respect to the illuminating wave l. The wave phase ϕ_{lj} may be written as

$$\phi_{lj} = \omega_l t - kr + k\vec{x}_j \cdot (\hat{r} - \hat{s}_l) \quad , \tag{2.3}$$

where

- ω_l is the illuminating beam angular frequency,
- $\vec{x}_j$ is the position of the jth particle with respect to the coordinate system origin,
- $\hat{r}$ is a unit vector in the direction of $\vec{r}$, and
- $\hat{s}_l$ is a unit vector in the direction of propagation of the illuminating wave.

The meanings of the various vectors and coordinates are shown in Fig. 2.3.

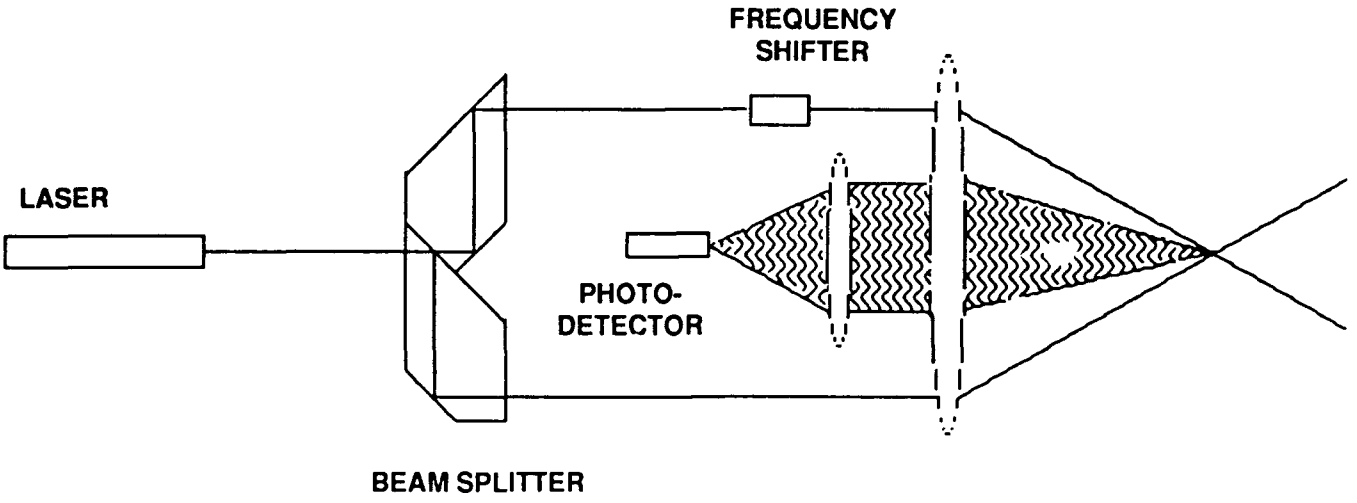

(a) DIFFERENTIAL OR DUAL-BEAM ARRANGEMENT

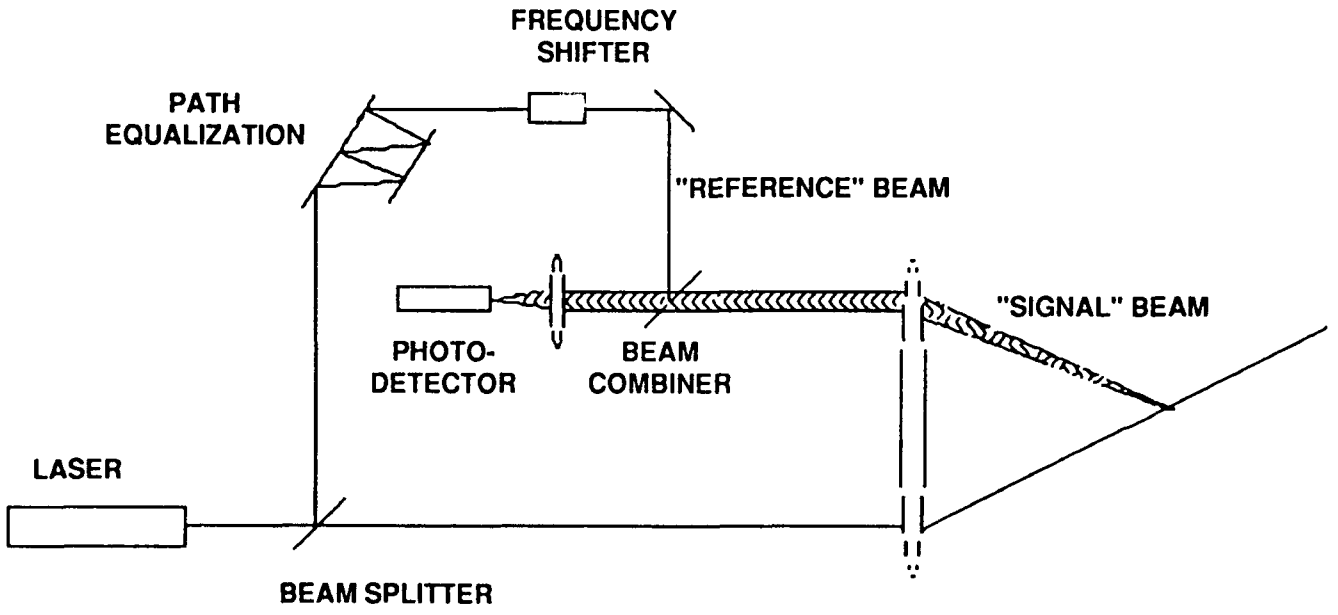

(b) REFERENCE BEAM ARRANGEMENT

FIGURE 2.2
SCHEMATIC LDV OPTICAL ARRANGEMENTS

ARL:UT
AS-90-822
MLB - DS
11 - 2 - 90

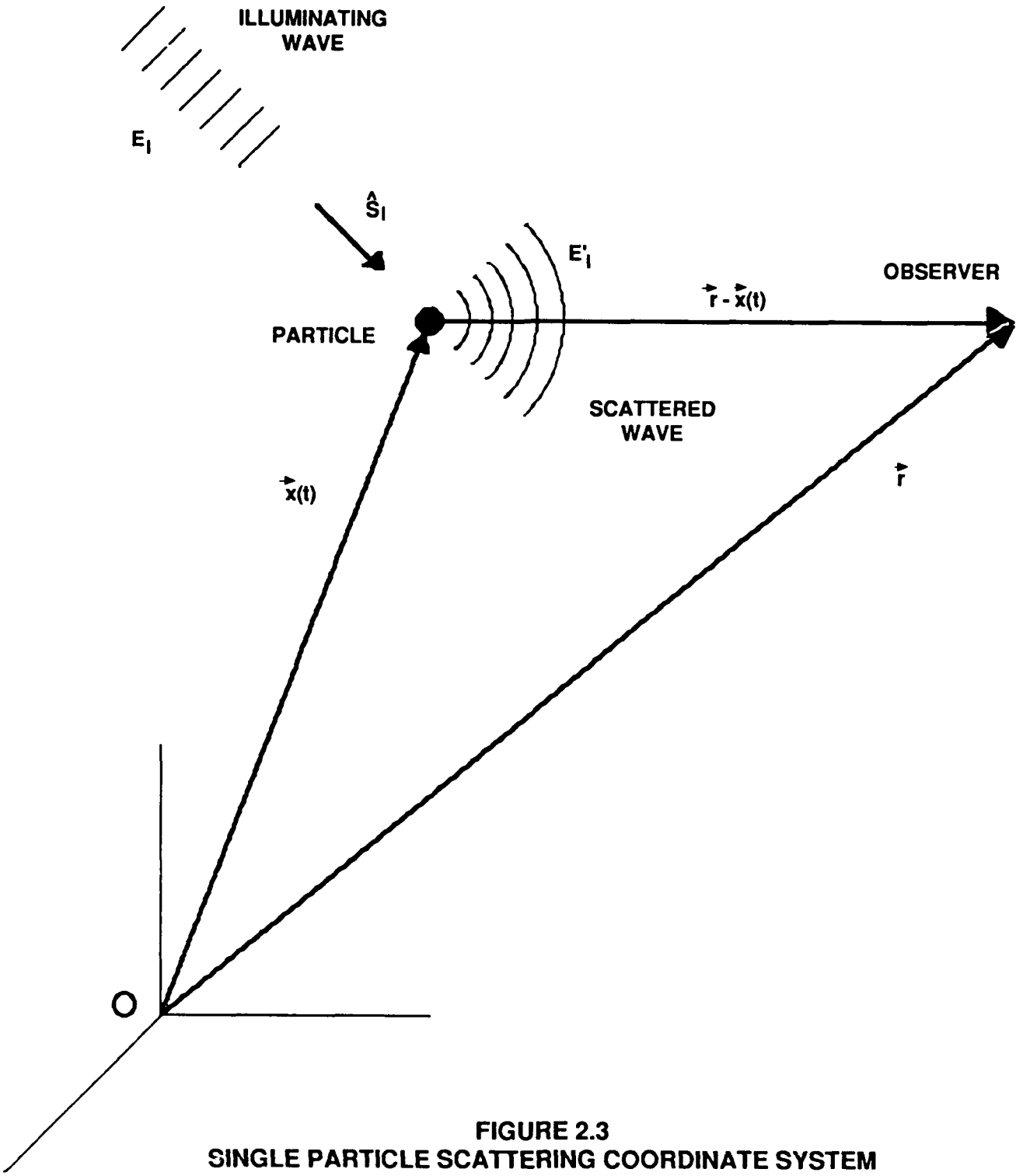

FIGURE 2.3
SINGLE PARTICLE SCATTERING COORDINATE SYSTEM

ARL:UT
AS-90-823
MLB - DS
11 - 2 - 90

In arriving at the above expressions, several assumptions have been made (1) that the observer is in the farfield (i.e., that the distance $|\vec{r}|$ is much greater than both the wavelength of the light and the scatterer diameter), and (2) that $|\vec{x}_j|<<|\vec{r}|$. The second assumption implies that $\vec{r}$ and $\vec{r}-\vec{x}_j$ are nearly parallel and that the scattered spherical wave may be represented as diverging from the origin.

The relationship between the scattered wave phase and the Doppler shift may be obtained by noting that the instantaneous angular frequency is the time derivative of the phase

$$\dot{\phi}_{lj} = \frac{\partial \phi}{\partial t} = \omega_l + k\,\vec{v}_j \bullet (\hat{r} - \hat{s}_l) \quad . \tag{2.4}$$

In the above expression $\vec{v}_j \bullet \hat{r}$ is the Doppler term associated with the particle's velocity component toward the observer, while $-\vec{v}_j \bullet \hat{s}_l$ is associated with the scatterer's motion away from the illuminating wave. Thus the total frequency shift depends linearly on the velocity component in the $\hat{r}$-$\hat{s}_l$ direction.

2.2 DIFFERENTIAL OR DUAL-BEAM LDV SIGNAL

Using the above results, the form of the signal for the differential LDV configuration may now be derived. In both this and the reference beam arrangement, light from two beams is combined (mixed) at a photodetector. Because a photodetector is a "square law" device, the output of the photodetector is proportional to the real part (since a complex wave representation is used) of the square of the total electric field incident on the detector. Assuming a single scatterer and using the above results, the intensity per unit area at the photodetector can be written as[9]

$$I = I_1 \frac{\vec{\sigma}_{1j} \bullet \vec{\sigma}_{1j}^{*}}{(kr)^2} + I_2 \frac{\vec{\sigma}_{2j} \bullet \vec{\sigma}_{2j}^{*}}{(kr)^2} + \frac{2\sqrt{I_1 I_2}}{(kr)^2} \mathrm{Re}\left[\vec{\sigma}_{1j} \bullet \vec{\sigma}_{2j}^{*}\, e^{i(\phi_{1j} - \phi_{2j})}\right] \quad , \tag{2.5}$$

where the subscripts 1 and 2 refer to illuminating beams 1 and 2, respectively. The first two terms in the expression are due to light scattering from each beam

individually, while the last term (which is the Doppler signal) results from interference (mixing) of the light from the two beams. As is standard practice[9] in LDV systems of this type, it is assumed that one of the illuminating beams is frequency modulated at frequency ω_B. Using Eq. (2.3), we may evaluate the phase dependence of the Doppler term in the above equation obtaining

$$\phi_{1j} - \phi_{2j} = \omega_B t + k\vec{x}_j \bullet (\hat{s}_2 - \hat{s}_1) \quad . \tag{2.6}$$

This expression indicates that for the differential LDV configuration, the Doppler shift is associated with the scatterer velocity in the $\hat{s}_2$-$\hat{s}_1$ direction, which lies in the plane of the illuminating beams and is perpendicular to the bisector of the angle between the beams.

In order to simplify the expression for the intensity at the photodetector given by Eq. (2.5) above, it is assumed that the illuminating beams are of equal intensity (i.e., that the scatterer is near the center of the region of beam intersection) and that the scattering coefficients are equal for each beam (which is reasonable when the detector is positioned near the line defined by the illuminating beams bisector). The intensity per unit area is now integrated at the detector over the detector aperture and the following is obtained.

$$I(t) = \int_{\Omega} I\, r^2\, d\Omega = A_j\left(1 + \cos\left(\phi_{1j} - \phi_{2j}\right)\right) \quad . \tag{2.7}$$

The coefficient, A_j, contains the dependence on the illuminating intensity and the scattering dynamics. In the above expression, the integrated phase shift resulting from phase angle differences between E'_1 and E'_2 is arbitrarily set to zero. The intensity at the detector may then be written as

$$I(t) = A_j\left(1 + \cos\left(\omega_B t + \left(\frac{4\pi}{\lambda}\sin\kappa\right)X(t)\right)\right) \tag{2.8}$$

by utilizing Eq. (2.6) and expressing the displacement in the $\hat{s}_2$-$\hat{s}_1$ direction as

$$\vec{x}_j \bullet (\hat{s}_2 - \hat{s}_1) = 2\, X(t) \sin\kappa \quad . \tag{2.9}$$

Here X(t) is the displacement amplitude in the $\hat{s}_2$-$\hat{s}_1$ direction and κ is the half-angle between the two laser beams.

Assuming the scatterer's motion is periodic with angular frequency ω_a, the displacement in the $\hat{s}_2$-$\hat{s}_1$ direction can be written as

$$X(t) = X_a \sin \omega_a t \quad . \tag{2.10}$$

The modulation index (m) is defined as

$$m = \frac{4\pi}{\lambda} X_a \sin \kappa \quad , \tag{2.11}$$

and the intensity at the photodetector is written as

$$I(t) = A_j (1 + \cos (\omega_B t + m \sin \omega_a t)) \quad . \tag{2.12}$$

Using trigonometric identities and Fourier series expansions, this may be rewritten[10] as

$$I(t) = A_j + A_j \langle J_0(m) \cos \omega_B t - J_1(m)[\cos (\omega_B - \omega_a) t - \cos (\omega_B + \omega_a) t]$$

$$+ J_2(m)[\cos (\omega_B - 2\omega_a) t + \cos (\omega_B + 2\omega_a) t] - \cdots \rangle \quad , \tag{2.13}$$

where J_n are Bessel functions of the first kind. Equation (2.13) represents the general form of the differential LDV signal under the conditions and approximations given above.

2.3 REFERENCE BEAM LDV SIGNAL

For the reference beam LDV system, a development similar to that for the dual-beam can be followed. In the reference beam configuration, the optics are arranged such that the "reference" beam is collinear with the "scattered" beam at the detector. The intensity per unit area at the detector (assuming a single scatterer) is given by

$$I = I_1 \frac{\vec{\sigma}_{1j} \cdot \vec{\sigma}^*_{1j}}{(k\,r)^2} + \frac{I_2}{(k\,r)^2} + \frac{2\sqrt{I_1 I_2}}{(k\,r)^2} \mathrm{Re}\left[(\vec{\sigma}_{1j} \cdot \hat{p}_2)\, e^{i(\phi_{1j} - \phi_2)}\right] \quad , \quad (2.14)$$

where

$I_1(I_2)$ is the illuminating intensity of the scattered (reference) beam,

σ_{1j} is the scattering coefficient for the jth particle illuminated by the scattering beam, and

$\hat{p}_2$ is the unit polarization vector of the reference beam.

The phase of the Doppler term in the above expression can be evaluated in a manner similar to what was done for the differential configuration and yields the same result (Eq. (2.6)). However, because of the requirement that the reference beam be collinear with the scattered beam at the detector, this implies $\hat{s}_2 = \hat{r}$ and means that the reference beam configuration is sensitive to the scatterer velocity component in the $\hat{r} - \hat{s}_1$ direction.

Following the development of the differential system, one can assume that the reference beam is frequency modulated, and can integrate over the detector aperture, define a modulation index, and make the same simplifying approximations, except for the assumption that the two detected beams are of equal intensity. The resulting intensity at the photodetector may be written as

$$I(t) = I_{1j} + I_2 + 2\sqrt{I_{1j} I_2} \cos(\omega_B t + m \sin \omega_a t) \quad , \quad (2.15)$$

where the symbols have the same meanings as in the previous development, except that I_2 is the intensity of the reference beam. Again, one can use trigonometric relations and Fourier series expansions to rewrite this as

$$I(t) = I_{1j} + I_2 + 2\sqrt{I_{1j} I_2} \langle J_0(m)\cos \omega_B t - J_1(m)[\cos(\omega_B - \omega_a)\, t - \cos(\omega_B + \omega_a)\, t]$$

$$+ J_2(m)[\cos(\omega_B - 2\omega_a)\, t + \cos(\omega_B + 2\omega_a)\, t] - \cdots \rangle \quad . \quad (2.16)$$

It is worth restating here that the modulation index (m) is equal to $(4\pi/\lambda)$ $(X_a \sin\kappa)$ except that for the reference beam arrangement, X_a is the displacement amplitude in the $(\hat{r} - \hat{s}_1)$ direction and κ is the half-angle between

the incident "scattering" beam and the "virtual" incident illuminating beam, which is collinear with $\vec{r}$.

3. LDV SIGNAL SIMULATION

3.1 GENERAL

In order to investigate the effects of various noise sources on signal detectability under the approximated conditions discussed in the previous section, a computer program has been developed for generating a simulated LDV signal. In this section the general features of the computer model will be presented. Results obtained using this model are given in the following sections.

To develop the computer model, it was necessary to apply certain "constraints" to the system to be simulated. It was assumed that the LDV system would be used in a backscatter configuration (monostatic transceiver) and that there would be no artificial enhancement (seeding) of the fluid (seawater) scattering characteristics. These considerations, together with the modest laser powers which would likely be used in any initial test of such a system, led to the conclusion that the detected light intensity would be weak enough to be photon-resolved. Therefore the signal generation algorithm has been constructed around this premise.

An additional constraint for our model is that only a single acoustic tone of angular frequency ω_a is allowed. Under this assumption, the Doppler signal appears as sidebands around a carrier frequency ω_B and the modulation index (m), which is the argument of the Bessel function weighting coefficients, determines the relative amplitudes of the carrier and sidebands.

The simulated signal generation begins by representing the light intensity at the photodetector as a function given by Eq. (2.12) (differential) or Eq. (2.15) (reference beam). These forms are slightly modified to allow noise parameters to be specified as part of the signal. Noise parameters are provided to allow for random variations in the phase of the Doppler term and additive random noise to the total signal over specified ranges (a provision is also made for adding phase noise to the demodulation process if the signal is to be basebanded). The assumed functional forms for the detected intensities are

$$I(t) = \left[1 + \cos\left(\omega_B t + m \sin\left(\omega_a t + \xi\right) + \phi_n\right)\right] + n(t) \qquad (3.1)$$

for the differential configuration and

$$I(t) = \left[1 + R + 2\sqrt{R} \cos\left(\omega_B t + m \sin\left(\omega_a t + \xi\right) + \phi_n\right)\right] + n(t) \qquad (3.2)$$

for the reference beam configuration. In the above equations ξ is a random starting phase for the acoustic waveform, ϕ_n is a random phase noise parameter, n(t) is an additive random noise parameter and, for the reference beam, R is the ratio I_2/I_1 of the reference beam intensity to the scattered beam intensity. The user supplied inputs include the acoustic frequency ω_a, the sampling frequency, the total sample time, the laser modulation frequency ω_B, the modulation index (m), and the mean number of detected photons per second. If the various noise parameters are to be used, the user also specifies the allowed range of variation for each random variable.

Once the light intensity envelope as given by the above equations has been specified and calculated at each sample point, the envelope is normalized to the mean number of detected photons per second and the number of detected photons per sample period calculated. A photon shot noise contribution to the signal is then simulated using a random number generator which provides a Poisson distribution about the mean number of photons in each sample period. The program output is a series of numbers representing the number of detected photons per sample period over some specified length of time.

3.2 LIMITATIONS OF THE LDV SIGNAL SIMULATIONS

The modeled LDV signal program developed contains many of the characteristics which are expected in an actual LDV signal; however, there are certain features of LDV signals which have not been modeled. Although it is believed that the model reproduces the signal characteristics which are most relevant to an investigation of improved signal processing techniques, it is worth noting the limitations of the model and the known differences between the modeled signal and an actual signal.

It is presumed in our model that the signal originates from the motion of a single scatterer and that the scattering center is located near the center of the measurement volume. In an actual measurement, more than one scatterer may be present in the measurement volume simultaneously and these may be located anywhere within the volume. Further, an actual signal would probably not be continuous, but would occur in "bursts" as particles enter and leave the measurement volume. One consequence of these conditions is the reduction of the optical coherence of the Doppler signal due to phase differences in the light scattered from the different particles at different locations in the measurement volume. In addition, a data acquisition system might not acquire data continuously, but rather collect data only when a particle was present in the measurement volume using some form of data acquisition triggering scheme.

It is also assumed in our model that the motions of the scattering centers are dominated by those produced by the acoustic field. In an actual measurement, Brownian motion and local fluctuations in the physical characteristics of the seawater would contribute to the scatterers' motions. A known effect of these additional motions is the broadening of the Doppler frequency[1] associated with an acoustic tone. Also, when multiple particles are present in the measurement volume, Brownian motion may cause partial or complete decorrelation of the signals originating from the various scattering centers and can limit the minimum frequency one is able to sense if the frequencies of interest are less than the decorrelation frequency due to Brownian motion.[1]

As evidenced by the discussion above, our model generates a somewhat simplified form of the LDV signal. However, it is believed that the signal properties most important to developing improved signal processing algorithms have been incorporated. Further enhancements to the model may be warranted once prospective signal processing techniques have been identified. For the present, the limitations of our model should be kept in mind when assessing possible advantages and disadvantages of any signal processing technique.

4. POWER SPECTRAL PROCESSING STUDIES OF LDV SIGNALS

4.1 EFFECTS OF NOISE ON SIGNAL "DETECTABILITY"

As a first step in understanding the limiting factors in employing LDV systems as remote acoustic sensors, we conducted an empirical investigation of Doppler signal detectability using our modeled LDV signal and power spectral processing techniques. In the model, we assumed that the particle motion is dominated by that produced by a single acoustic tone and therefore we can relate the particle motion to the properties of the acoustic field. For an acoustic plane wave of angular frequency ω_a, the acoustic displacement is related to the sound pressure[11] as

$$X_a = \frac{P}{(\rho_a c)\,\omega_a} \quad . \tag{4.1}$$

Here P is the acoustic SPL of the tone and $\rho_a c$ is the specific acoustic impedance of the medium. Since the above expression actually describes the displacement of "particles" of the fluid medium, an implicit assumption has been made here that the motions of the scattering centers follow the fluid motions. This is expected to be a valid assumption for the ranges of frequencies and particle sizes we are interested in.[1] To set a scale for the acoustic displacements measurable with an LDV system one can examine the laboratory results reported in the literature. Acoustically driven displacements of order 10^{-7} - 10^{-8} m have been measured in water;[1,2,4] the corresponding range of the modulation index (which determines the carrier to sideband amplitude ratio) for the configurations used is approximately 0.1 - 1.0 radian. For an LDV-based underwater acoustic sensor to be of tactical value, these sensitivities would need to be extended a minimum of 1 or 2 orders of magnitude (m = 0.01 - 0.001 radian).

Efforts to establish sensitivities of an LDV system to various noise sources began by investigating a "minimal noise" system in which the only noise source was due to radiation noise (photon shot noise). It can be shown[12] that for a Poisson distribution, which describes discrete processes such as

photodetection, the signal-to-noise ratio present in the incident signal is given by $(\bar{n})^{1/2}$, where $\bar{n}$ is the mean number of incident photons in some time period T. Thus for a noiseless detector system where only radiation noise is present, there will be some minimum photon flux which must impinge on the photodetector for a given Doppler signal strength. Based on this observation we conducted a study of LDV signal detectability (here defined as a visual identification of the Doppler sidebands in a power spectrum) as a function of detected photon flux for both the differential and reference beam arrangements. Since the differential LDV system is the configuration most often used in LDV measurements and the simpler of the two to implement optically, our analysis will center primarily on this form of LDV signal. However, when notable differences in the results exist for the two arrangements, attention will also be given to the reference beam system.

In the noise studies presented here, the signal processing consisted of demodulation of the signal at the carrier frequency (ω_B) and computation of an autocorrelation function and power spectrum. The computation of the power spectrum from the autocorrelation was chosen because this method has been demonstrated to provide good signal detectability when photon fluxes are low enough to be photon-resolved.[13] The results of the shot noise study are presented graphically in Fig. 4.1, where the minimum photon fluxes (detected photons per second) necessary to visually identify the Doppler sidebands are given as a function of modulation index (m) for power spectra computed from a single 1 s record (triangles) and for ensemble averaged (ten records) power spectra (squares). Typical ensemble averaged power spectra for two different incident photon fluxes and a modulation index of 0.01 radian are shown in Fig. 4.2. As seen in Fig. 4.1, both the single record and averaged power spectral methods show a smooth dependence between the minimum photon flux and the modulation index and the general feature that higher detected photon fluxes are required as the Doppler signal amplitude decreases. In addition, some "processing gain" is seen for the ensemble averaged power spectra, as expected.

Similar results were obtained for the reference beam configuration as a function of modulation index. However, due to the different geometries of the differential and reference beam arrangements, an acoustic tone of a given SPL

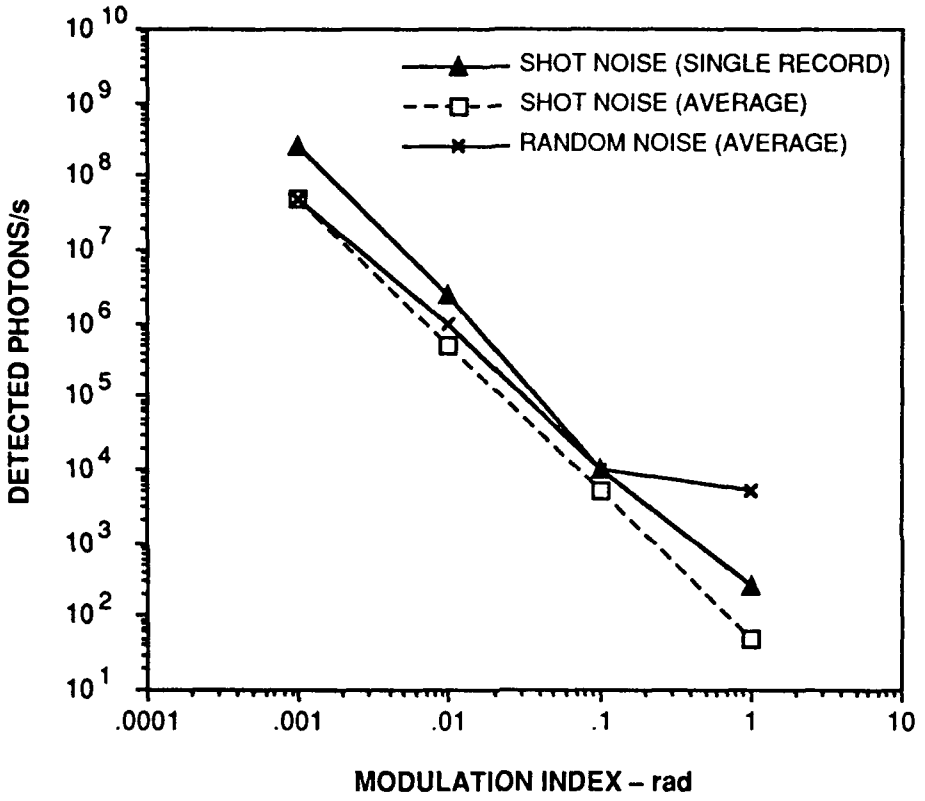

FIGURE 4.1
EFFECTS OF NOISE ON THE MINIMUM PHOTON FLUX REQUIRED FOR DOPPLER SIGNAL DETECTABILITY

The results of an empirical study of the effects of noise on the minimum detected photon flux for Doppler signal detectability in a power spectrum. The results are based on a modeled LDV signal and are discussed in detail in the text. The curves shown in the figure serve as a visual guide only and do not represent the results of calculations.

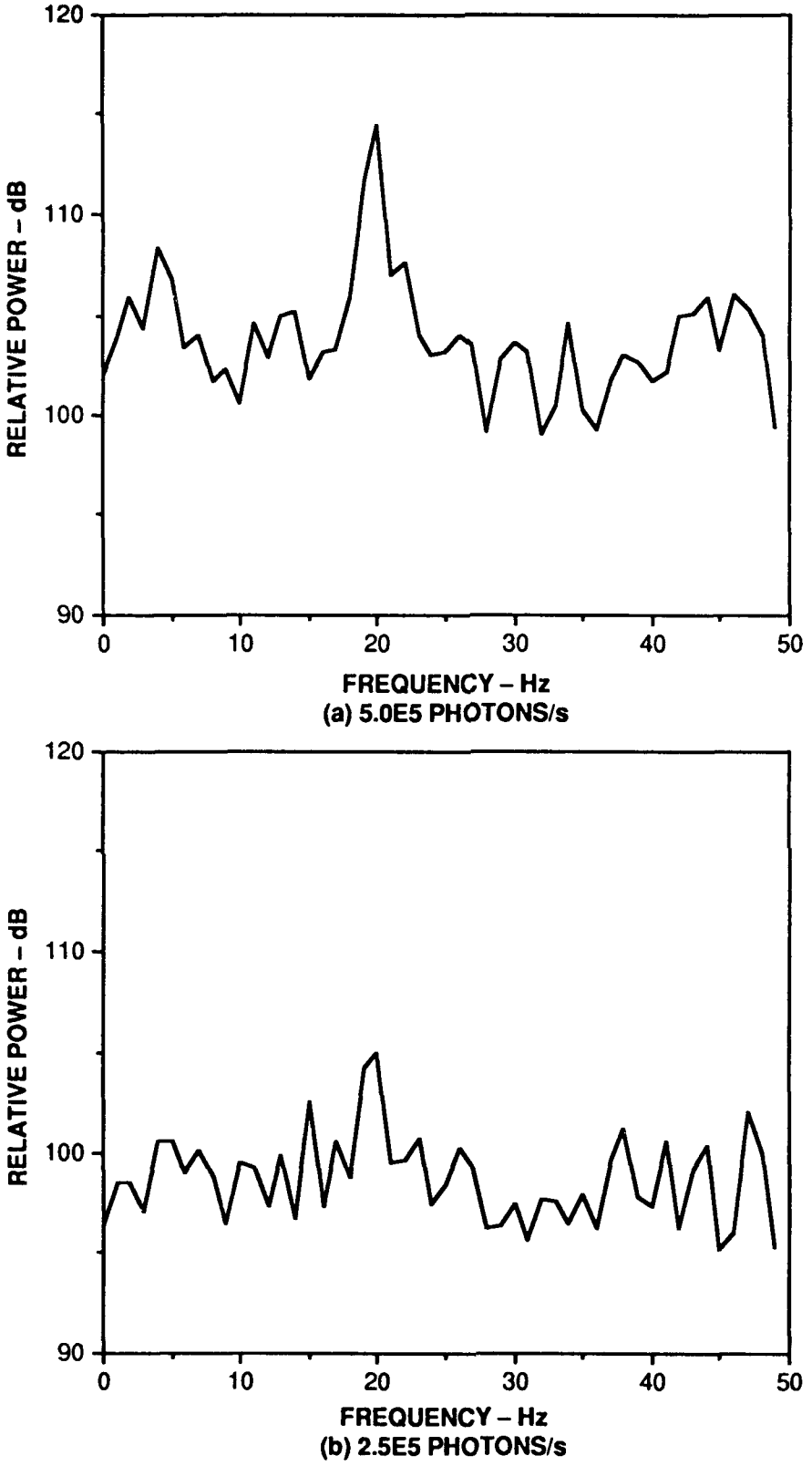

FIGURE 4.2
EFFECT OF DETECTED PHOTON FLUX ON DOPPLER SIGNAL VISIBILITY

Power spectra resulting from a 10-record incoherent average of modeled LDV signals with the modulation index set to 0.01 rad. The figure shows the effect of detected photon flux on visual signal identification of the Doppler peak at approximately 20 Hz.

ARL:UT
AS-90-825
MLB - DS
11 - 2 - 90

may produce a larger phase modulation for the reference beam system and thus may require fewer detected photons for identification of the sidebands at any given intensity of the acoustic field (the occurrence of these larger phase modulations depends on the orientation of the direction of LDV sensitivity with respect to the direction of propagation of the local sound field). It should also be noted that the limits obtained in this study are a function of the assumed processing scheme and are not absolute limits; different signal processing algorithms might alter these limits significantly.

After establishing the approximate minimum photon flux requirement as a function of modulation index for a "noiseless" system, we conducted an investigation of the sensitivities of signal detectability to the various noise sources built into our model. The model noise sources include a random noise term which may be added to the envelope of the intensity at the detector, a random phase noise term which may be included in the Doppler term of the signal, and a random phase noise which may be incorporated in the demodulation process. A set of runs was conducted to determine the approximate upper limits of the various noise sources as a function of modulation index when the detected photon flux was well above (typically 10^8 - 10^9 photons per second) the shot noise dominated minimum photon flux. Based on the results of these runs, limits for the maximum tolerable noise levels of each of the sources were inferred. It was found that maximum tolerable noise levels scaled more or less linearly with the relative sideband (Doppler signal) to carrier ratio, with weaker Doppler signals requiring lower noise levels to be detectable. In general, when a signal was not dominated by shot noise, the minimum signal-to-noise ratio for the additive noise associated with the intensity envelope was found to be about 1/M. Here M is a "dimensionless modulation index" and means, for example, that if one had a signal corresponding to a phase modulation (m) of 0.1 radians, then M=0.1 and the minimum signal-to-noise ratio for visual detection of the Doppler sidebands would be 1/M or 10 to 1. The maximum tolerable random phase noise associated with the Doppler term corresponded to about 0.1 m (a random phase noise of 0.01 radian for the above example) and the maximum random phase noise in the demodulation approached m (phase noise of 0.1 radian in the above case).

Although these limits are only approximate and are likely to vary for other signal processing schemes, the overall trends seen in this investigation have significant implications in an actual LDV-based acoustic sensor. First, detection of weak signals will only be possible (assuming the present, or a similar, power spectral technique is used) if the optical noise levels of the LDV system are small. This implies that a laser may need to be intensity-stabilized to reduce any intensity fluctuations to a tolerable level. Further, the elimination of potential sources of phase noise, both in the illuminating laser beams and the frequency shifting mechanism, appear to be critical. It is likely that these types of noise sources are limiting factors in current LDV-based acoustic sensor sensitivity.

Using the same processing scheme and the maximum noise level guidelines stated above, investigations were then made into the sensitivity of the LDV signal detectability to multiple noise sources. With the additive noise, phase noise, and demodulation noise present simultaneously, the minimum detected photon fluxes were determined for visual signal detectability; these values are represented by the x's of Fig. 4.1. The results indicate that when the Doppler signal is relatively strong (large modulation indices), noise levels well above the "shot noise limit" may be tolerated provided a sufficient number of photons are detected per unit time. As the modulation index and the corresponding Doppler signal amplitude become smaller, there is greater susceptibility to noise and eventually the overall tolerable noise levels approach those of a shot noise limited system. As stated earlier, it is clear from these results that the detection of acoustic fields at low intensities using LDV techniques will require a very quiet LDV and detector system and/or a signal processing method which provides maximal discrimination against any noise source present.

Finally, studies were made of the effect of varying the reference beam to signal beam intensity ratio on the Doppler sideband detectability for the reference beam arrangement. In principle, the reference beam intensity at the beam combiner (see Fig. 2.2) can be increased until the photon noise of the reference beam exceeds all other noise sources, thus optimizing the signal detectability.[1] Analysis of the simulated reference beam signals indicated that enhanced signal-to-noise ratios could be achieved in this manner. However,

when both the reference and scattered beams were allowed to contain additive random noise, the random fluctuations of the reference beam intensity limited the signal detectability when the reference beam intensity became too great. In general, reference beam to signal beam intensity ratios between 1 and 10 seemed to provide the optimal signal-to-noise ratios in the presence of the additive noise. The flexibility to adjust this ratio is one significant advantage of the reference beam arrangement and may under certain conditions (e.g., low scattered light intensities and stable laser illumination) allow better sensitivity to be obtained than is possible with the differential arrangement.

4.2 POWER SPECTRAL COMPARISON BETWEEN SIMULATED AND ACTUAL LDV SIGNALS

As a means of validating the results obtained using our simulated LDV signal, a small data sample from an LDV measurement of an acoustic tone in a standing wave tube was analyzed.[14] The data were collected using a differential LDV system in a forward scattering arrangement as described in Ref. 2. The sampling rate was set to 200 kHz and the laser modulation frequency to approximately 50 kHz. The data set consists of 16384 samples, representing slightly less than 0.1 s of data. The acoustic tone had a frequency of approximately 1810 Hz and an SPL of 180 dB re 1 μPa, corresponding to a modulation index of 0.33 radian. The photomultiplier signal was passband filtered (35 kHz to 65 kHz) and amplified (53 dB) prior to digitization.

A power spectrum was computed for the data set by segmenting the time series into 16 records and ensemble averaging the spectra. The result is shown in Fig. 4.3. A peak at the carrier frequency and sideband peaks at the carrier-acoustic sum and difference frequencies are readily evident in the spectrum. For comparison, an ensemble averaged power spectrum for a simulated LDV signal is shown in Fig. 4.4. This signal was generated for a modulation index of 0.33 radian and a mean detected photon flux of 10^7 photons per second. Random phase noise was limited to 0.03 radian and the signal-to-noise ratio for the additive noise term was set to 10 to approximate the carrier peak to broadband background ratio seen in the power spectrum of the LDV data.

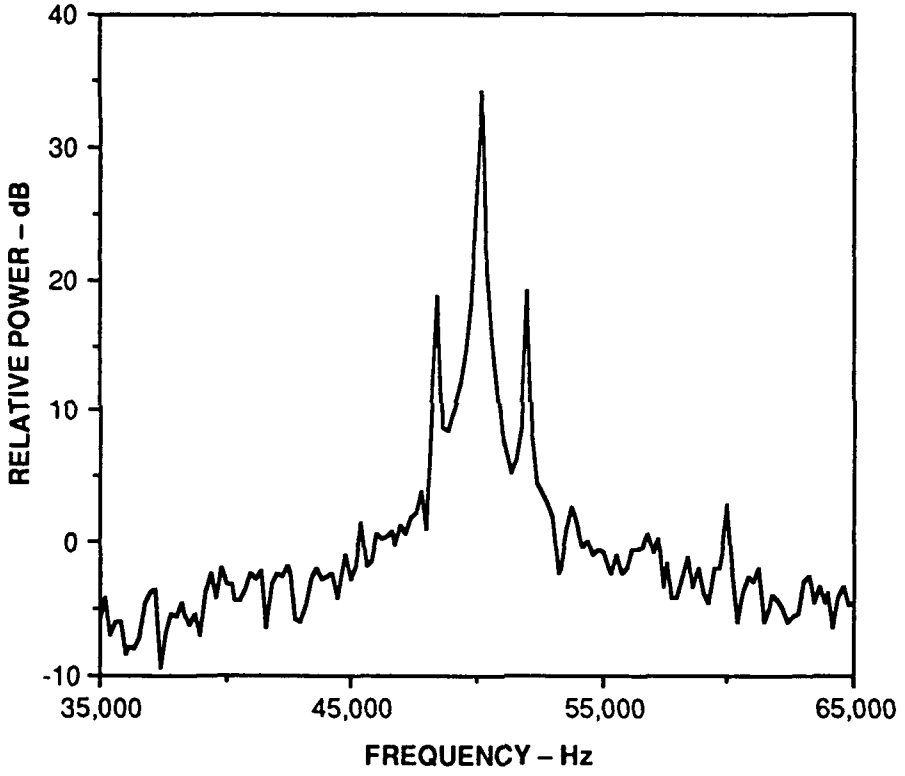

FIGURE 4.3
POWER SPECTRUM FROM AN ACTUAL LDV MEASUREMENT

The spectrum consists of a 50 kHz carrier peak with sideband lobes at approximately ±1810 Hz above and below the carrier. The modulation index for this signal is approximately 0.33 rad. The spectrum was obtained from an incoherent average of 16 records. (Ref. 14)

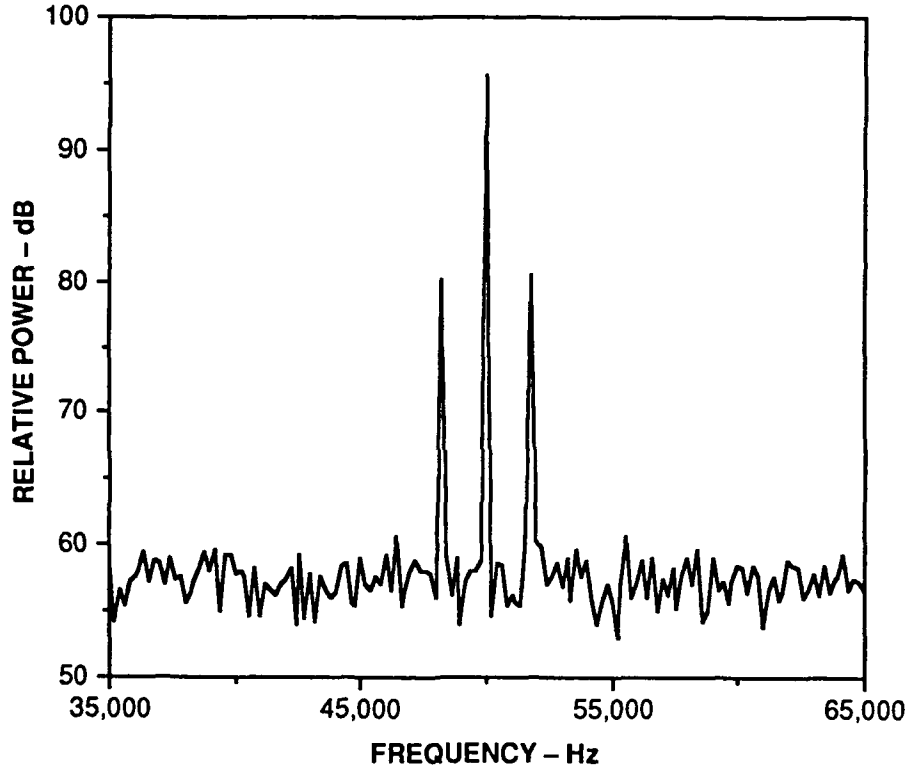

FIGURE 4.4
POWER SPECTRUM FROM A SIMULATED LDV SIGNAL

The signal was generated for a modulation index of 0.33 rad and an additive random noise signal-to-noise ratio of 10, as discussed in the text. The spectrum shown is the result of a 16-record incoherent average.

The most obvious difference between the two spectra is the lack of peak broadening in the power spectrum of the simulated signal, as discussed previously. In addition, the LDV power spectrum has a slightly asymmetric background and has a shape which is suggestive of a broad structure centered near the carrier frequency. Other features of the two spectra, such as the carrier to sideband amplitude ratio and the overall signal-to-noise ratio of the narrowband peaks and broadband background, appear to be in good agreement. Since it is these features which normally dominate the ability to identify the Doppler sidebands, it is believed that the simulated signals provide reasonable approximations of actual LDV signals. (It should be noted that spectral broadening does affect the capability to resolve the carrier and sidebands and thus is expected to limit the minimum detectable frequency. This issue has not been addressed in this study.) The ability to control the various noise contributions to the simulated signal as well as the capability to vary the various signal parameters over a wide range makes the use of a simulated signal attractive for studies of potential LDV signal processing schemes.

5. CALCULATIONS OF SCATTERED PHOTON FLUXES FOR LDV SYSTEMS

This section focuses on the potential limitations of LDV-based remote acoustic sensing when the sensor is employed in a backscatter configuration and the acoustic medium is seawater. Because the number of photons arriving at the photodetector will ultimately limit the dynamic range of an LDV sensor, it is appropriate to consider how particular LDV optical configurations are related to the photon flux at the photodetector. "Standard" backscatter configurations for both the differential and reference beam arrangements will be considered; optical parameters which are appropriate for laboratory-based measurements have been chosen. Some considerations for employing an LDV sensor in the field (open ocean) will follow.

The scattered photon flux may be expressed in terms of the initial photon flux for an attenuating medium as[1]

$$I' = I\, e^{-2\alpha r}\, \beta(\theta)\, L\, d\Omega \quad , \tag{5.1}$$

where

- I' is the scattered photon flux,
- I is the initial photon flux entering the medium (source photon flux),
- r is the distance between the scattering volume and the point where I' is determined,
- α is the attenuation coefficient of the medium through which the photons propagate,
- $\beta(\theta)$ is the scattering function of the medium,
- L is the length of the scattering volume as seen by the detector, and
- $d\Omega$ is the solid angle over which the scattered light is detected.

Here it is assumed that the transmitter (laser) and receiver (photodetector) are at the same distance r from the scattering volume. It should be noted that the above expression does not account for several mechanisms which may affect the actual detected photon flux. Among these are the detector efficiency (quantum efficiency), losses at optical interfaces, and background light and/or flare (optical reverberation) incident on the detector.

The parameters which determine the scattered flux in terms of the initial flux may be grouped into two categories: those which depend on the properties of the medium [α, $\beta(\theta)$] and those which depend on the optical arrangement (r, L, $d\Omega$). Since we will consider a laboratory arrangement for an LDV sensor, any attenuation caused by the medium will be ignored and we will set the attenuation coefficient to zero. The implications of attenuation will be discussed later in this section. The scattering function $\beta(\theta)$ characterizes the scattering process and is a function of the scattering angle θ, the optical properties of the medium (which is assumed to be seawater) and, to a lesser extent, the wavelength of the illuminating radiation. There have been many studies of the scattering characteristics of seawater, and general features of the seawater scattering function are well documented.[15,16] Perhaps the most significant feature for our particular application is the angular dependence of the scattering function, where one finds a rapid falloff of scattered flux as the scattering angle increases. A minimum in the scattered light intensity typically exists near $\theta=100^{\circ}$-120° and the scattering function tends to rise somewhat at back angles. However, the backward scattering flux is still typically 2 to 3 orders of magnitude less than the scattered flux at forward angles. This implies that for the backscatter configuration assumed for our LDV system, one can expect substantially fewer photons to reach the photodetector than if one employed a forward scatter geometry.

For the purpose of obtaining estimates of the scattered photon flux for the LDV configurations under consideration here, it is necessary to assume a value for $\beta(\approx 180^{\circ})$. The scattering of light by seawater is produced by both scattering from the water itself and scattering from suspended particulates (hydrosols), but because the Doppler signal is dominated by light scattered from moving hydrosols, focus will be on the particulate scattering properties of seawater. Studies of particulate scattering[16,17] suggest that a reasonable value of the scattering function for backscattering would be of the order 5×10^{-4} $(\text{m-steradian})^{-1}$ and this value has been adopted for our calculations. However, measurements[18,19] of particles sizes and concentrations at various geographic locations and depths show that large variations in seawater particulate properties exist and it is expected that these variations will manifest themselves as fluctuations in the scattered photon flux. The performance of an LDV

acoustic sensor may therefore depend upon the location at which it is operated. In addition, since LDV measurements are usually obtained from a small region of a fluid and "particle discreteness" (i.e., signal "bursts" due to particles entering and leaving the measurement volume) is commonly seen in the observed signal, the applicability of the general scattering properties of seawater discussed above is uncertain. In order to address these concerns, we are conducting a supplementary experimental program which is described in an appendix to this report.

To complete the specification of the parameters which relate the scattered photon flux to the initial photon flux, specific optical geometries for the differential and reference beam configurations are assumed. It is common practice in LDV backscatter configurations to use a single lens for focusing of the illuminating beam(s) and collecting the light from the measurement volume.[20] A schematic of the assumed optical geometries at this transceiver lens is shown in Fig. 5.1 for the differential arrangement, and in Fig. 5.2 for the reference beam system. In the differential configuration, the two parallel beams incident on the transceiver lens are focused and intersect at the focal point of the lens. Backscattered light from the measurement volume is collected over the central region of the lens and may then be focused with additional optics (not shown) onto a photodetector. The dual-beam configuration has the advantage that the observed Doppler shift is independent of the angle of observation and thus permits a large aperture to be used for collection of the scattered light.[20] For our assumed reference beam arrangement, only one beam enters the fluid and the scattered light is mixed with an external reference beam (not shown) after passing through the transceiver lens. The measurement volume for this configuration is defined by the intersection of the illuminating beam and the detector "beam" (the detected scattered light beam), which in our configuration is assumed to have the same spatial dimensions as the illuminating beam. The light collection aperture of the reference beam system is constrained to be the same as the area subtended by the illuminating beam at the transceiver lens to ensure that the collected light is coherent with

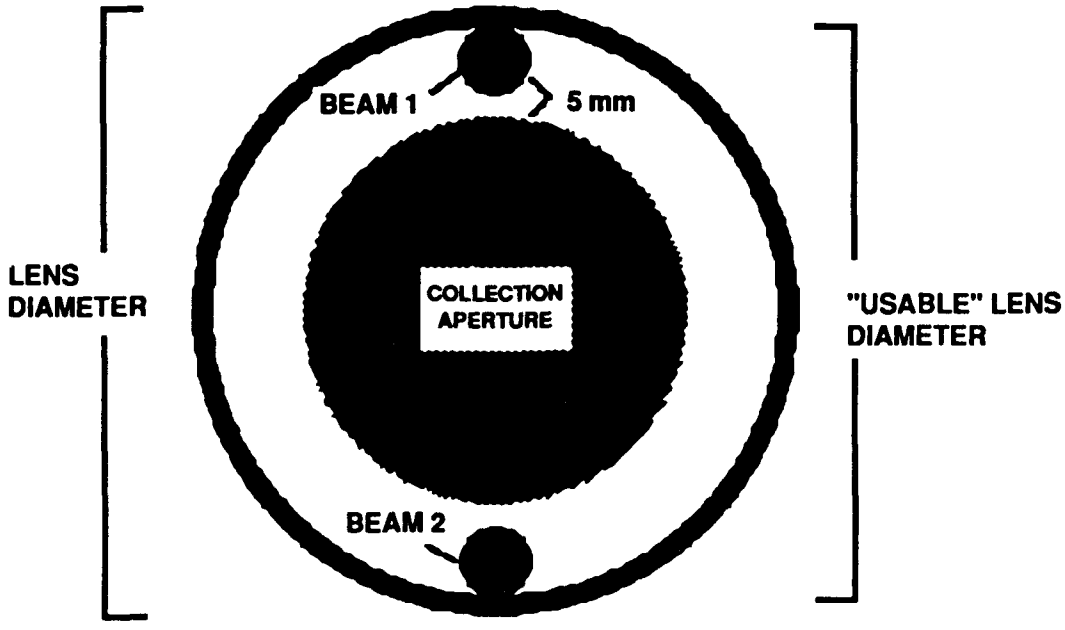

(a) FRONT VIEW

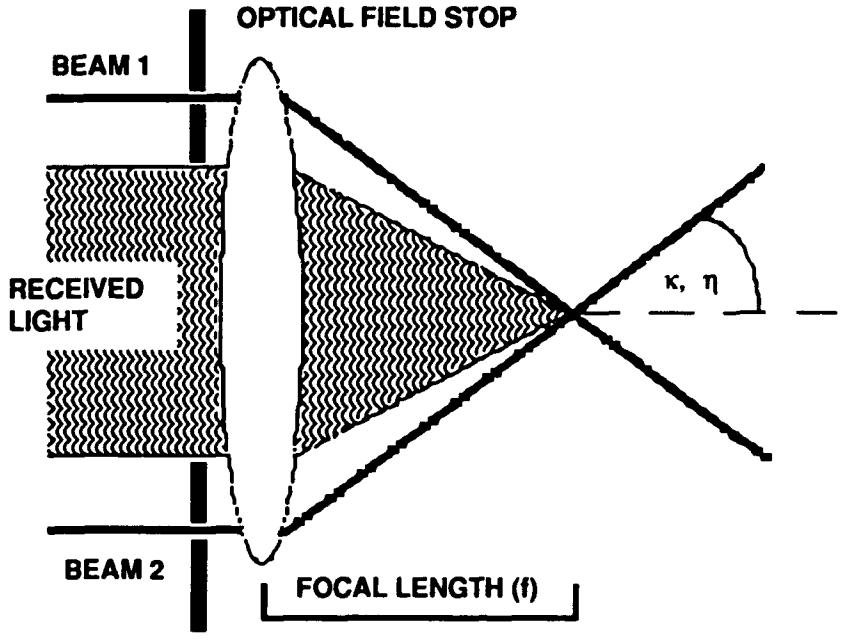

(b) SIDE VIEW

FIGURE 5.1
DIFFERENTIAL LDV TRANSCEIVER LENS GEOMETRY

Schematic views of the assumed optical geometry at the transceiver lens for the differential LDV arrangement. This geometry was used in calculating the dependence of the scattered photon flux on the various optical parameters, as discussed in the text.

ARL:UT
AS-90-828
MLB - DS
11 - 2 - 90

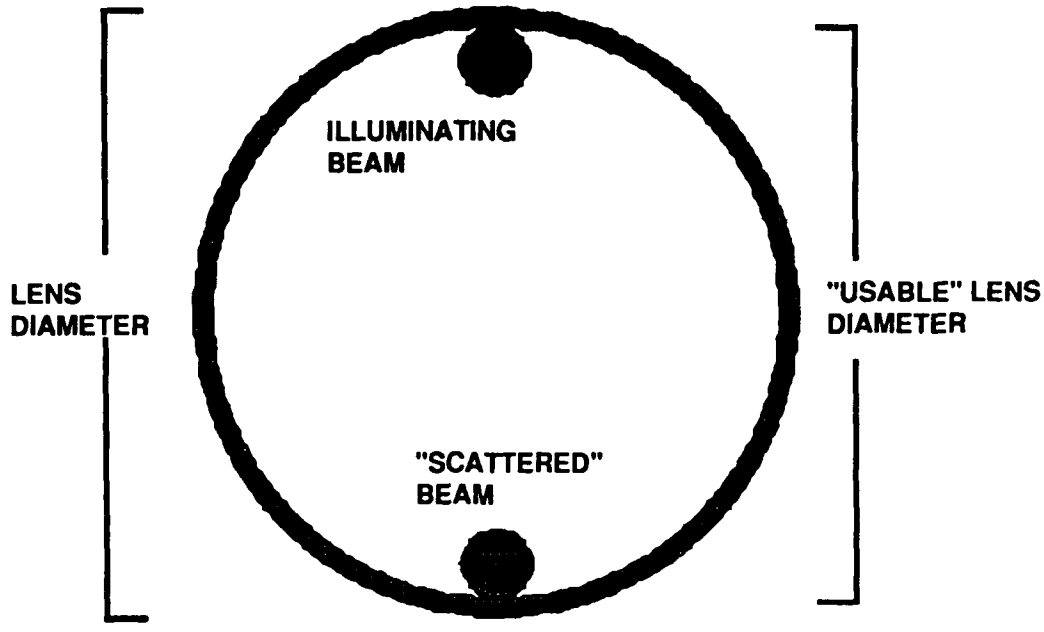

(a) FRONT VIEW

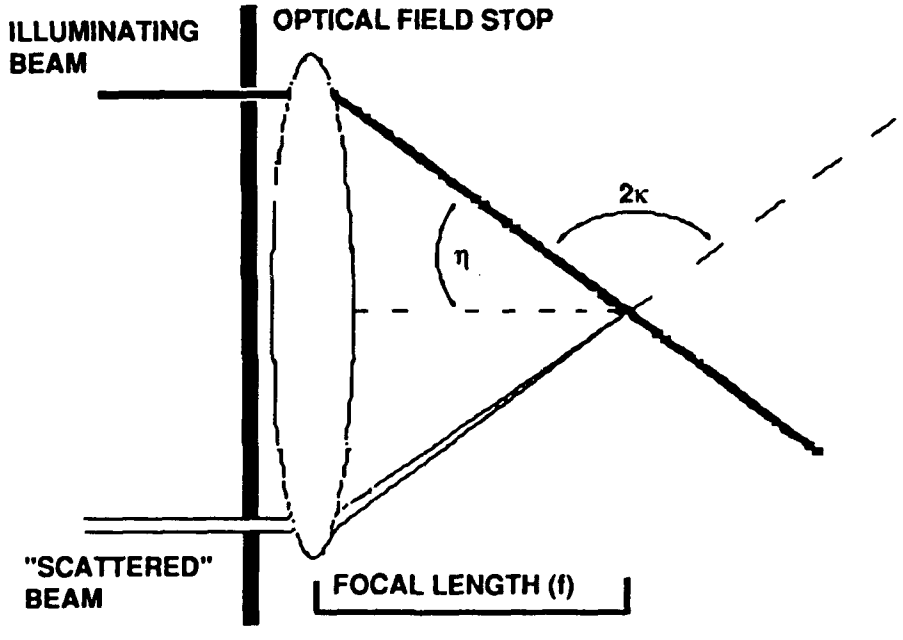

(b) SIDE VIEW

FIGURE 5.2
REFERENCE BEAM LDV TRANSCEIVER LENS GEOMETRY

Schematic views of the assumed optical geometry at the transceiver lens for the reference beam LDV arrangement. This geometry was used in calculating the dependence of the scattered photon flux on the various optical parameters, as discussed in the text.

ARL:UT
AS-90-838
MLB - DS
11 - 2 - 90

the reference beam.[9,20] This feature is one of the principal drawbacks of the reference beam configuration. This disadvantage is somewhat offset by the larger phase modulation (modulation index) which may be produced by a given particle motion if the system is oriented in the optimal direction with respect to the motion. It should be noted that beam expansion is often employed in reference beam systems because expansion of the illuminating beam prior to passing through the transceiver lens produces both a smaller waist at the focus and a correspondingly smaller measurement volume. This, in turn, permits one to collect light over a larger aperture and still meet coherence criteria.

Given the above configurations, the remaining parameters (r, L, $d\Omega$) may be calculated in terms of various optical parameters such as the transceiver lens diameter and focal length and the diameter of the illuminating beam(s) at the transceiver lens. Our scattered flux calculations use values for the various optical parameters which could realistically be implemented in a laboratory setup. We have considered transceiver lens focal lengths from 200 to 1000 mm and lens diameters from 50 to 200 mm. The usable lens diameter was assumed to be 80% of the actual lens diameter. (This minimizes the effects of optical aberrations which often become severe near the edges of optics elements.) The initial laser beam diameter, defined as the diameter at which the intensity has fallen to $1/e^2$ of its centerline value, was taken as 1.25 mm and is a typical value for an off-the-shelf ion laser. Beam expansion factors of up to 10X were also considered in the calculations.

The measurement volume defined by the intersecting beams (the two illuminating beams of the differential arrangement or the illuminating and detector beams of the reference beam arrangement) is ellipsoidal in shape and may be defined by the expression[9]

$$V_m = \frac{\pi\, d_{e^{-2}}^3}{6 \cos\eta \sin\eta} \quad . \tag{5.2}$$

Here $d_{e^{-2}}$ is the beam waist diameter at the focus and η is the half angle between the beams as shown in Figs. 5.1 and 5.2. The measurement volumes for the ranges of optical parameters cited above varied from approximately 2×10^{-9} m^3 to 3×10^{-15} m^3. The smallest values of the scattering volumes

considered here are probably not achievable in practice but were considered in this study for completeness.

A modest illuminating power of 5 mW was assumed at the measurement volume and calculations of the scattered photon flux were performed for various combinations of the optical parameters. For the reference beam arrangement, it was found that the detected scattered flux was maximized with maximal beam expansion (10X) and that the scattered flux was almost independent of the lens focal length. The dependence on beam expansion is the direct result of having to satisfy a coherence criteria and the fact that smaller measurement volumes permit larger apertures of coherence.[20] The lack of variation with focal length is due to an elongation of the measurement volume as the focal length increases and the detection solid angle decreases. For the differential arrangement, larger lens diameters (and thus larger detection apertures) were found to enhance the photon flux at the detector. However, beam expansion was found to have the opposite effect for the differential arrangement, primarily because of the decrease in the size of the measurement volume. Again, there was little sensitivity to the lens focal length due to the competing effects of the increasing length of the scattering volume and the decreasing detection solid angle as the focal length increases. For both configurations it was found that when one used the optimal optical geometry and the value for the seawater scattering function given previously, a sufficient number of photons reached the detection aperture to allow demonstrated LDV-based acoustic sensor sensitivities to be extended several orders of magnitude if the system is shot-noise limited. If additional noise sources are present, the LDV sensor sensitivity would be correspondingly reduced, as discussed in the previous section of this report. Since the assumed power at the measurement volume for these calculations was only 5 mW, more intense illuminating beam(s) may allow reasonable LDV sensitivities to be achieved in noisier systems.

Finally, if deployment of an LDV-based acoustic sensor in the open ocean is considered, one must account for the effect of attenuation on the scattered photon flux reaching a detector aperture. Attenuation of light by seawater is the result of both absorption and scattering processes and the attenuation coefficient (α of Eq. (5.1)) exhibits a substantial dependence on wavelength as well as geographic variations at a given wavelength. For the

wavelengths of electromagnetic radiation presently available from lasers, seawater is most transparent in the visible region of the spectrum (400-700 nm) and exhibits minimum absorption near 480 nm.[15] Representative attenuation lengths $1/\alpha$ for this region of the electromagnetic spectrum are 20-30 m.[1,15,16] Sensing of acoustic fields at a distance will require the propagation of both the illuminating beam(s) and the scattered light through seawater, and substantial (>85%) scattered light flux will be lost due to attenuation when measurement distances are on the order of one attenuation length away from the LDV system. Thus, although it may be possible to construct LDV sensors with high initial beam intensities, the effective range of remote sensors will probably be limited to modest distances due to attenuation losses. In addition, an LDV system used in an ocean environment will require data acquisition and signal processing systems which are able to function for a range of scattered photon fluxes due to the variability of the physical properties of seawater with location and depth.

6. HIGHER ORDER PROCESSING TECHNIQUES

An examination of the forms of the LDV signals given by Eq. (2.13) (differential arrangement) and Eq. (2.16) (reference beam arrangement) reveals that the signals contain harmonic structures which are manifested as sidebands about a central carrier frequency. The harmonic character of the LDV signal (photodetector output) has been "exploited" in several laboratory demonstrations by using higher order processing techniques (specifically, bispectral processing).[21,22] The results of these measurements indicate that higher order processing techniques may provide a level of discrimination against various noise sources which cannot be obtained from more conventional processing techniques such as power spectral analysis. Since the results given in the previous sections of this report show that the various noise sources included in our modeled LDV signal reduce and/or limit the visual detectability of the Doppler peaks in the power spectra of these signals, we have begun a study of higher order spectral processing techniques for use with an LDV-based acoustic sensor. The results of an initial investigation of several higher order processing techniques are presented in this section.

As a first step in evaluating higher order processing techniques for our particular application (i.e., remote acoustic sensing using LDV techniques), one must consider which of the various techniques are applicable for processing signals of the form one anticipates with our LDV signal model. For our modeled signal, only a single acoustic tone has been considered, and focus is on the detection of weak acoustic fields, where the sideband to carrier amplitude ratios are small. Under these conditions one generally finds values for the modulation index m which are much less than 1 (radian), and the harmonic series given by Eq. (2.13) or (2.16) reduces to a waveform containing only the carrier and first order sideband frequencies.[1] Since a nonvanishing bispectrum requires a degree of coherence (or specific phase relationships) between a triplet of frequencies ω_1, ω_2, and $\omega_1+\omega_2$,[23] our modeled signal is not expected to have a bispectral signature under the conditions discussed above. However, certain nonstationary processing functions, such as the co-intensity or spectral correlation, depend only on coherences between pairs of frequencies (e.g., the carrier and first sideband frequencies) and our investigation of potential higher order processing techniques has begun by using these.

In establishing an estimation technique for the co-intensity, the procedure outlined by O'Donnell[24] will be followed. A more formal treatment of the spectral correlation function for cyclostationary processes has been given by Gardner[25] and summarized by Baugh[26] and will not be repeated here. It is assumed that there is a nonstationary, real, discrete uniformly sampled time series x(n) of length N and with Fourier transform $X(f_j)$. The frequencies f_j are restricted to values less than or equal to $\pm f_N$, where f_N is the Nyquist frequency for the sampled time series. The spectral correlation function for any pair of fixed frequencies f_i and f_j is given by the expression

$$S_{xx}(f_i,f_j) = E\left[X(f_i)\, X^*(f_j) \right] \quad , \tag{6.1}$$

where E represents the expectation value and the * denotes the complex conjugate. It is readily seen from the above expression that one obtains the power spectrum when the spectral correlation function is evaluated for values where $f_i = f_j$.

In general, the above function assumes values which depend on both the amplitudes of the frequency components and the phase relationships (coherence) between them. Because we are relying on the coherence between the carrier and Doppler sidebands to provide discrimination against the noise background, the dependence on amplitude in the above expression can be suppressed to provide a measure of phase coherence between spectral components. The resulting co-intensity function has the form

$$s^2(f_i,f_j) = \frac{|\, S_{xx}(f_i,f_j)\,|^2}{E\left[\,|X(f_i)|^2\right]\; E\left[\,|X(f_j)|^2\right]} \quad , \tag{6.2}$$

and is restricted to values $0 \le s^2 \le 1.0$. To obtain a consistent estimate of the co-intensity, one usually employs an averaging or smoothing process in the time or frequency domain and we have adopted a time averaging approach. Also, in order to provide a means of detecting either constant phases between spectral components or constant phase differences resulting from the interaction having a time varying phase,[24] the time averaging was done using phase differences

between adjacent records of the time series. In this approach it is assumed the Fourier amplitude is given as

$$X_d(f_j) = \frac{|X_n(f_j)| + |X_{n+1}(f_j)|}{2} e^{i(\phi_{n+1} - \phi_n)}, \quad (6.3)$$

where the subscripts n and n+1 refer to consecutive records. The spectral correlation and co-intensity functions are then computed from the above formulations using these complex "phase difference" Fourier components.

In order to evaluate the effectiveness of the co-intensity spectrum for visually detecting the Doppler sidebands, a series of calculations were performed using modeled LDV signals. To simplify both the calculations and display of the co-intensity, a routine was used which fixes one of the two dependent frequencies and computes the co-intensity as a function of the other frequency. The fixed frequency was generally assumed to be the laser modulation frequency since the sidebands should exhibit a degree of coherence with the carrier. In order to ensure that a reasonable statistical estimation of the co-intensity was obtained, 80-record ensemble averages were used for the calculations.

Shown in Fig. 6.1 are the ensemble averaged power spectrum and co-intensity function (computed at the laser modulation frequency) for a simulated LDV signal corresponding to a modulation index (m) of 0.001 radian. The signal was constructed by assuming a sampling rate of 200 Hz, a laser modulation frequency of 50 Hz, and an acoustic frequency of 19.392 Hz. The detected photon flux was taken as 5×10^7 photons per second, the phase noise was limited to 0.0001 radian, and a signal-to-noise ratio of 1000 was assumed for the additive noise term. These values correspond to the maximum tolerable noise levels as determined by the power spectral analysis study of Section 4.1 for a modulation index value of 0.001 radian. As seen from the power spectrum plot of Fig. 6.1, the Doppler sideband peaks are barely discernible at about 30.6 Hz and 69.4 Hz. However, the corresponding sideband peaks are clearly seen in the co-intensity plot. As further evidence that the phase information preserved in spectral correlation processing appears to provide increased

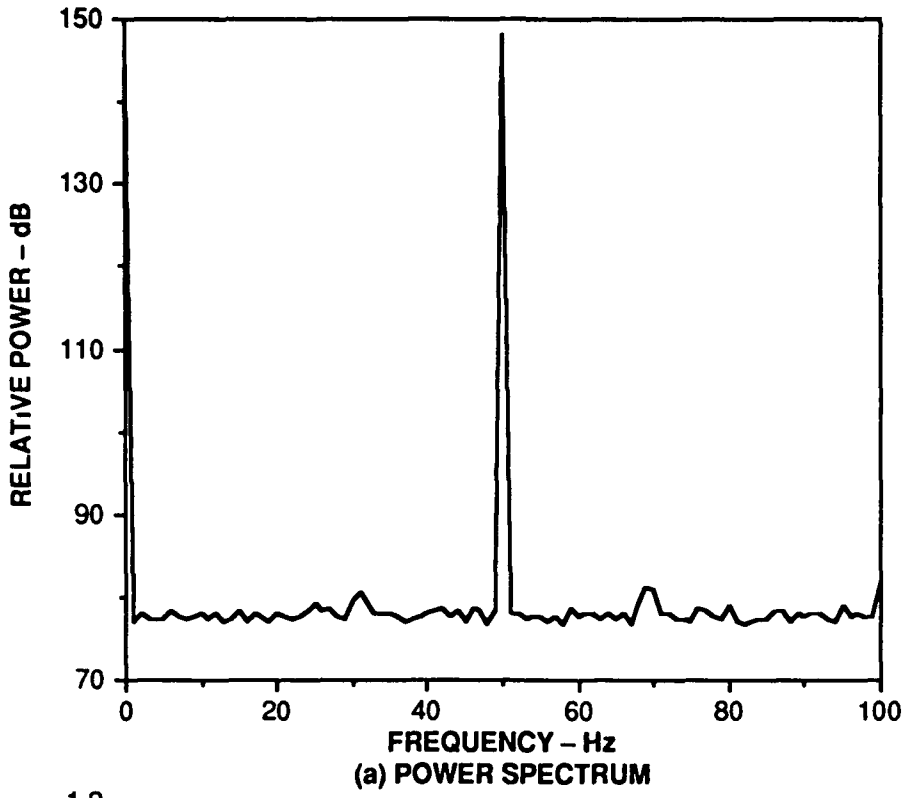

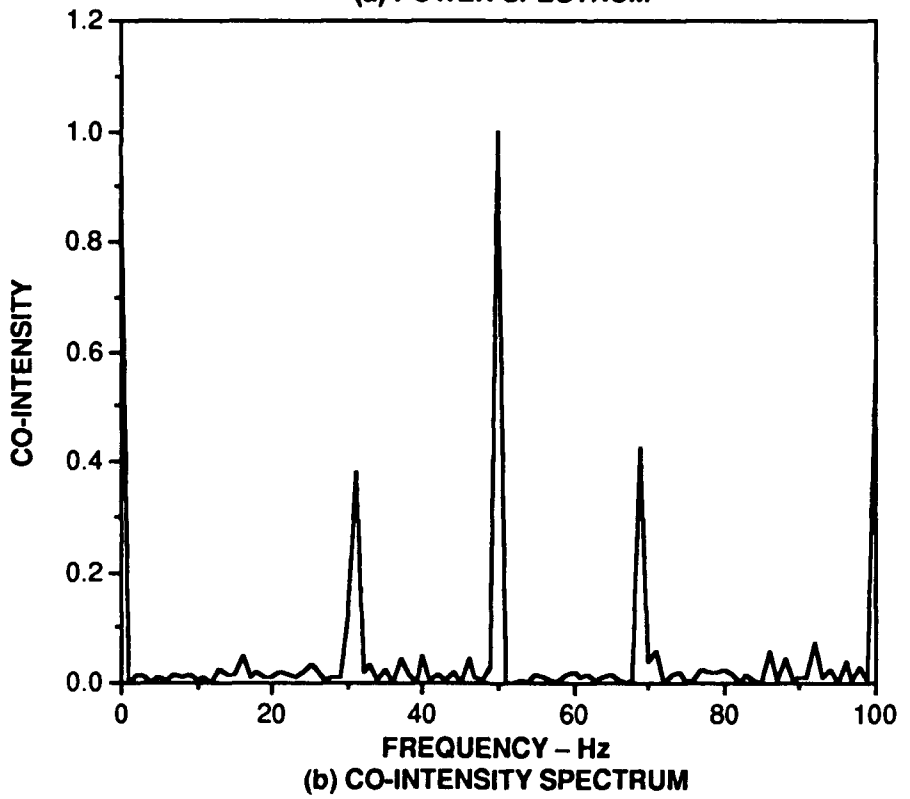

FIGURE 6.1
COMPARISON OF POWER AND CO-INTENSITY SPECTRA FOR A SIMULATED LDV SIGNAL

The power spectrum (a) and co-intensity spectrum (b) for a simulated LDV signal with a phase modulation value of 0.001 rad and a signal-to-noise ratio of 1000 for the random additive noise term. The co-intensity spectrum is displayed for one of the two dependent frequencies fixed at the carrier frequency of 50 Hz. The Doppler sidebands occur at approximately 30 Hz and 70 Hz. The power spectrum (co-intensity spectrum) is the result of an 80-record incoherent (coherent) average.

ARL:UT
AS-90-839
MLB - DS
11 - 2 - 90

signal detectability, another calculation was performed where the additive noise level was raised well above that of the previous calculation. For this calculation a signal-to-noise ratio of 400 was used for the additive noise term and all other parameters were held fixed. The results are shown in Fig. 6.2. The sideband peaks are no longer visible in the power spectrum, but the peaks remain easily identifiable in the co-intensity spectrum, although their degree of coherence with the carrier has been reduced.

Additional comparisons between power spectra and co-intensity spectra were performed over a wide range of noise levels and phase modulation values. In all cases, visual identification of the Doppler sidebands was enhanced for the spectral correlation processing compared with the power spectral processing as the noise levels were increased relative to a given signal strength. A more rigorous analysis will be required to quantitatively determine "processing gains" in the presence of various noise sources, but our initial investigation suggests that the Doppler sidebands may be detectable via spectral correlation processing at random noise levels which are approximately twice as large as the maximum tolerable levels obtained from the power spectral analysis.

As a means of providing an additional comparison between the simulated LDV signal and an actual LDV signal, the co-intensity for both the simulated and real LDV signals described in Section 4.2 was computed. The results are shown in Fig. 6.3 where the co-intensity for the actual LDV signal at a fixed frequency of 50.2 kHz (which corresponds to the center of the carrier peak) and the corresponding co-intensity for the simulated LDV signal are shown. Both spectra result from modulation index values of approximately 0.33 radian and have been averaged over 16 records, which was limited by the amount of real LDV data available for processing. As seen from the figure, the resulting spectra are quite similar. The "background" levels in the co-intensity spectra indicate that a larger data set is probably necessary to obtain spectra which are statistically converged, but in both spectra the carrier and sideband peaks are strongly evident.

From a comparison of the simulated and actual LDV co-intensities one sees a small decrease in coherence between the carrier and sidebands for the

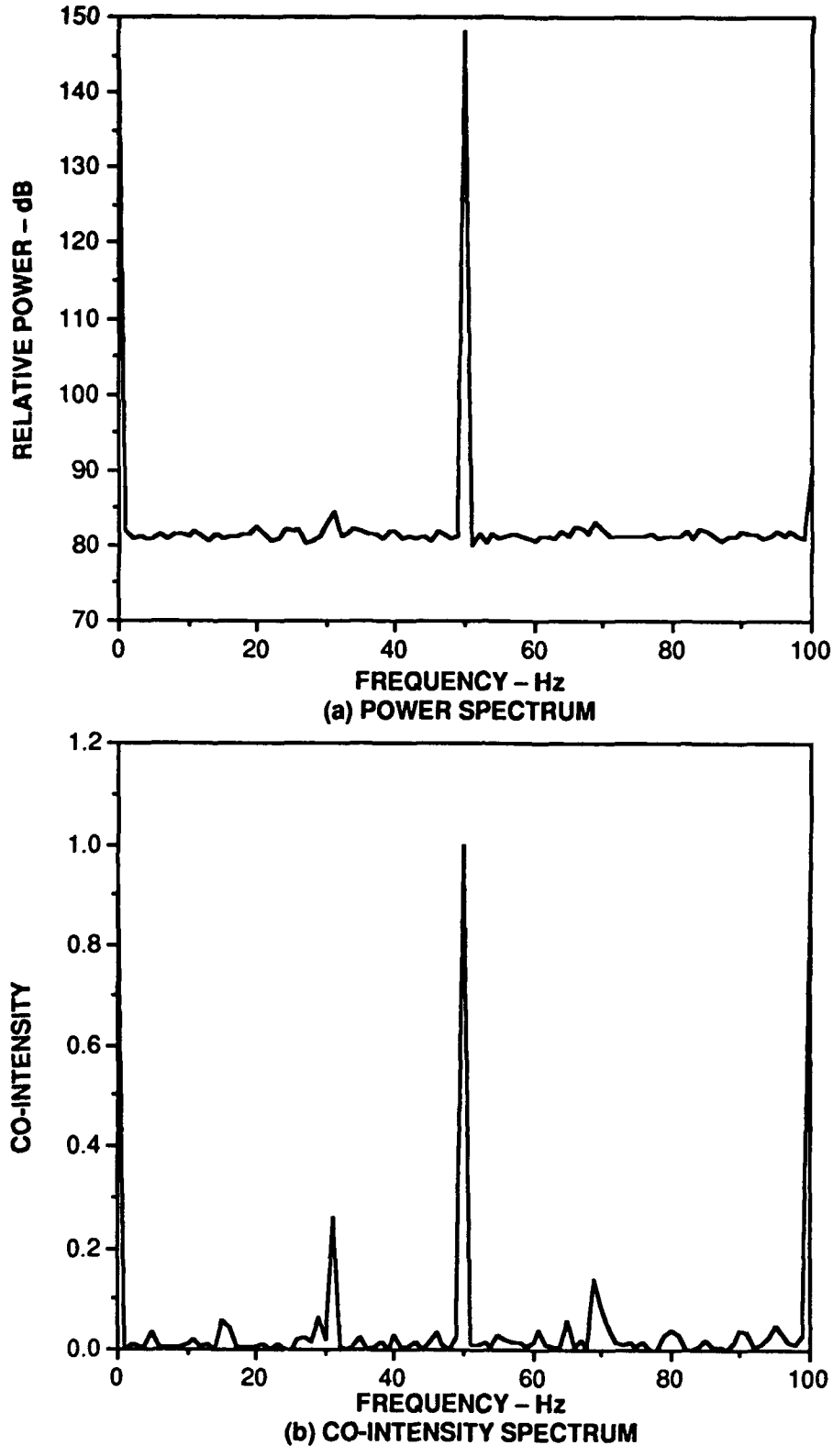

FIGURE 6.2
COMPARISON OF POWER AND CO-INTENSITY SPECTRA FOR A SIMULATED LDV SIGNAL WITH ADDITIONAL NOISE

The power spectrum (a) and co-intensity spectrum (b) for a simulated LDV signal with a phase modulation value of 0.001 rad and a signal-to-noise ratio of 400 for the random additive noise term. The co-intensity spectrum is displayed for one of the two dependent frequencies fixed at the carrier frequency of 50 Hz. The Doppler sidebands occur at approximately 30 Hz and 70 Hz. Both spectra are the result of 80-record averages. Incoherent (coherent) averaging was used to obtain the power spectrum (co-intensity spectrum).

ARL:UT
AS-90-840
MLB - DS
11 - 2 - 90

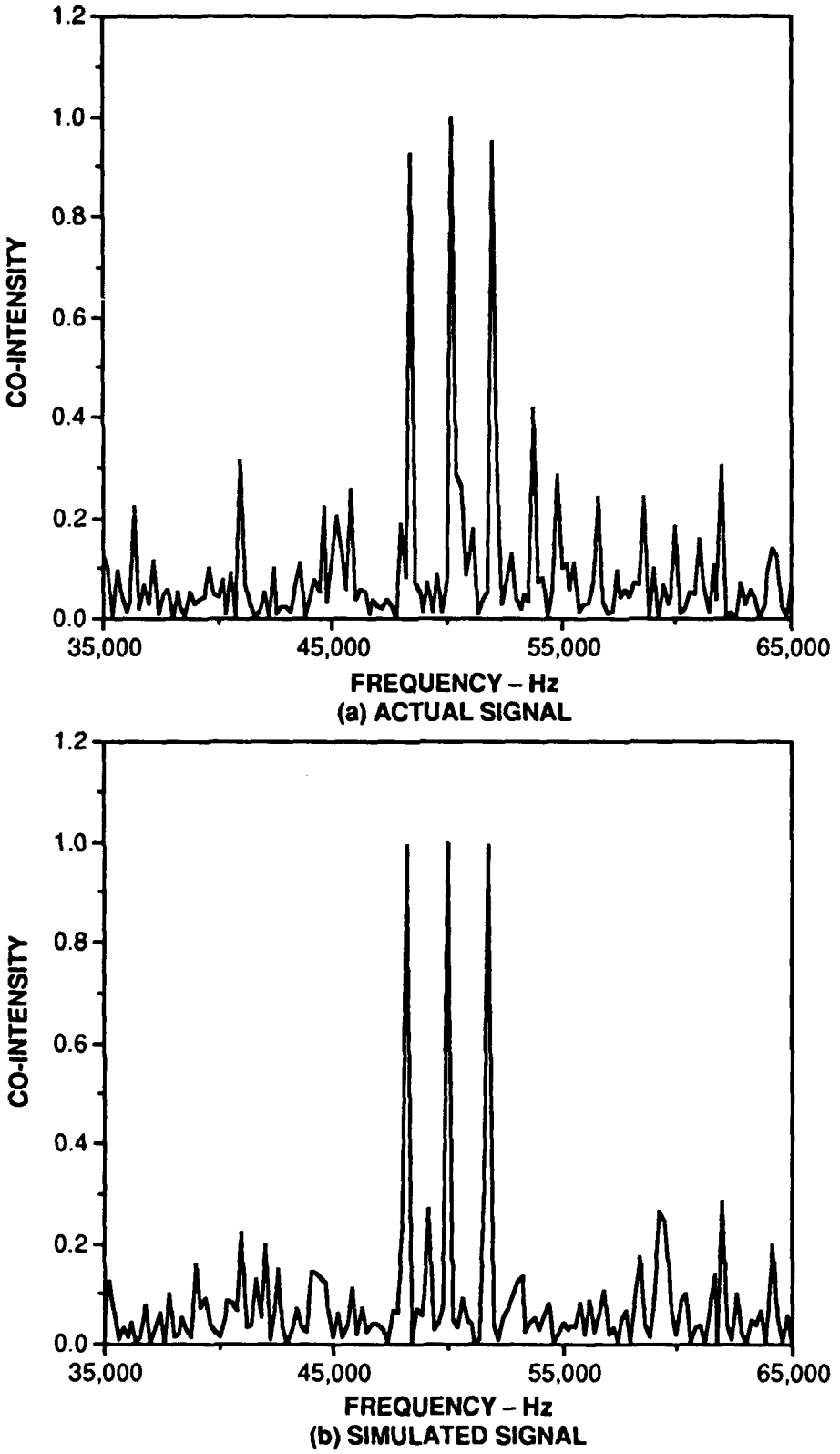

FIGURE 6.3
COMPARISON BETWEEN CO-INTENSITY SPECTRA FROM ACTUAL AND SIMULATED LDV SIGNALS

Co-intensity spectra for an actual LDV signal (a) and simulated signal (b) with phase modulation values of about 0.33 rad. The spectra are displayed for one of the two dependent frequencies fixed at the carrier frequency of about 50 kHz. The Doppler sidebands occur at approximately 1810 Hz above and below the carrier. The spectra are the result of 16-record coherent averages.

ARL:UT
AS-90-841
MLB - DS
11 - 2 - 90

real signal as compared to the simulated signal. There are a number of possible effects which may account for these differences. First, the spectral energy is more broadly distributed for the actual LDV signal, as evidenced by the wider carrier and sideband peaks observed in the power spectrum (see Fig. 4.3 of Section 4.2), and there appears to be a larger noise background under the carrier/sideband region of the actual LDV power spectrum. This may lead to reduced spectral coherence for specific frequency combinations such as those displayed in Fig. 6.3. Also, the actual signal may contain carrier phase noise (which is not included in the simulated signal) which may reduce the carrier-sideband coherence. Finally, the difference in coherence may be an artifact of the value we have chosen for the actual LDV carrier frequency (50.2 kHz) since possible values are constrained by the size of the fast Fourier transform used. In any case, differences of this order between the actual and simulated spectra are expected and are indicative of the physical processes and phenomena which have not been accounted for in the simulated signal.

As an extension of our initial investigation of spectral correlation processing, an attempt was made to find a modified processing scheme which would utilize the spectral symmetries found in this type of signal (i.e., a carrier with two side frequencies lying symmetrically above and below the carrier) in hope that it might produce additional processing gain in a noisy environment. The relationship of the carrier and sidebands may be most easily visualized using a vector interpretation of the modulation process.[27] If one begins with a form for the signal like that given by Eq. (2.13) for the differential LDV signal and assumes that the modulation index is small enough that only the first order sideband contributes to the signal, then the frequency dependent part of the signal may be written as

$$u(t) = \cos \omega_B t - \gamma[\cos(\omega_B - \omega_a)t - \cos(\omega_B + \omega_a)t] \quad . \qquad (6.4)$$

Here γ is the ratio $J_1(m)/J_0(m)$. For $m<<1$, one may approximate the values of the Bessel functions as $J_0(m) \approx 1$, $J_1(m) \approx m/2$, $J_2(m) \approx 0$, etc., and rewrite the above expression as

$$u(t) = \cos \omega_B t - \frac{m}{2}[\cos(\omega_B - \omega_a)t - \cos(\omega_B + \omega_a)t] \quad . \qquad (6.5)$$

If this expression is now converted to the complex phasor form, we obtain

$$u(t) = Re\left[e^{i\omega_B t}\left(1 - \frac{m}{2}e^{-i\omega_a t} + \frac{m}{2}e^{i\omega_a t}\right)\right] . \qquad (6.6)$$

If one ignores the term which has been factored out ($e^{i\omega_B t}$) and represents the constant rotation of the carrier unit vector at frequency ω_B in the counterclockwise direction, one may focus on the factor in parentheses which represents the modulation of the carrier. The three terms in this factor may be plotted as vectors in the complex plane[10] as shown in Fig. 6.4. The modulation is given by the resultant of these vectors. In the figure, the magnitude of the sideband vectors (m/2) has been exaggerated with respect to the unmodulated carrier vector for illustrative purposes. As seen from the figure, the resultant vector is rotated in phase but has almost the same amplitude as the unmodulated carrier, as expected for an FM signal. This occurs because the sum of the two sideband vectors is always normal to the unmodulated carrier (i.e., the sideband resultant is in phase quadrature with the unmodulated carrier).[10]

This relationship between the resultant sideband and carrier vectors has been adopted in a modified spectral correlation processing scheme. In this algorithm the spectral amplitudes are summed symmetrically about an assumed carrier frequency ω_c. Using the phase difference amplitudes of Eq. (6.3) will produce amplitudes of the form

$$X_F(\omega_c,\omega_i) = X_d(\omega_c), \left[X_d(\omega_c + n\,\Delta\omega) + X_d(\omega_c - n\,\Delta\omega)\right], \quad n=1,2,\ldots n_{max} \quad . \qquad (6.7)$$

The amplitudes are thus "folded" and summed about the specified carrier frequency. In the above expression $\Delta\omega$ is the frequency bin size (resolution) of the FFT used to generate the spectral amplitudes from the sampled time series. The number of folded amplitudes obtained using the above prescription is a function of where the specified carrier frequency lies in the frequency spectrum. The maximum number of amplitudes is obtained when ω_c is at the center of the spectral range and the number of folded frequencies which can be generated

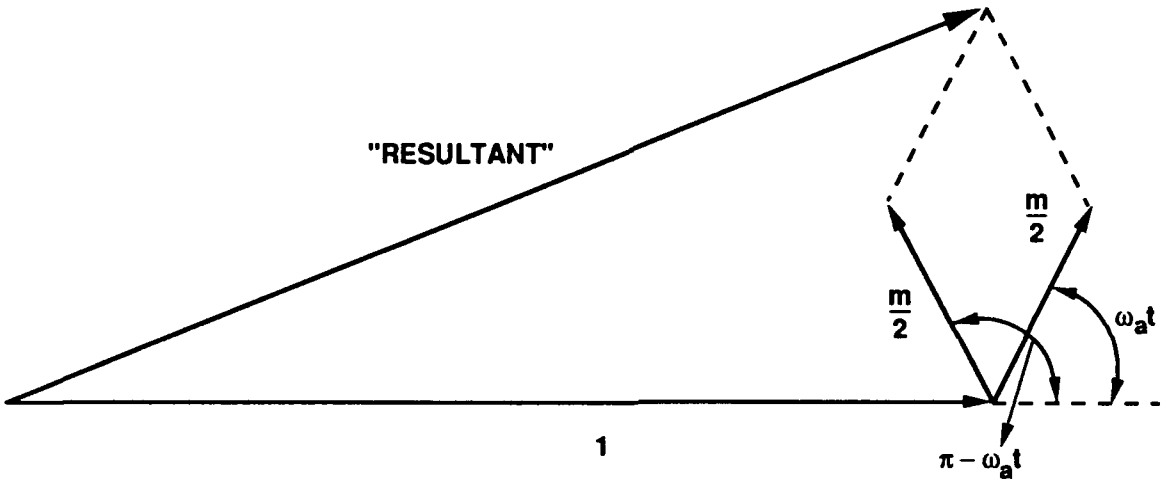

FIGURE 6.4
VECTOR DIAGRAM OF PHASE RELATIONSHIPS FOR LDV SIGNAL COMPONENTS

Vector diagram showing the relationship between the carrier and sideband phasors for an LDV signal, as discussed in the text. The magnitudes of the sideband phasors (m/2) are exaggerated for clarity in the figure.

ARL:UT
AS-90-842
MLB - DS
11 - 2 - 90

decreases as ω_c approaches the upper or lower frequency bounds of the spectrum.

Using the folded amplitudes, a co-intensity can then be computed using a method analogous to the one described above. In the following, a co-intensity computed from the folded amplitudes will be referenced as a "folded co-intensity" to distinguish it from the conventional co-intensity. It is worth noting at this point that the folded co-intensity has a principal domain which is reduced relative to the standard co-intensity domain. This is a manifestation of both the "folding" process and the dependence of the number of folded amplitudes for a given folding frequency on where the folding frequency lies in the spectrum. As in the case of the standard co-intensity, full two-dimensional functions will not be calculated and displayed, but rather the folded co-intensity with one of the two dependent frequencies fixed (in this case, at the folding frequency ω_c) will be presented. Practically, this is not an unreasonable approach since the laser modulation frequency will presumably be known in an actual measurement.

The results of a folded co-intensity calculation are shown in Fig. 6.5 for a folding frequency which was set to the laser modulation frequency. The spectrum represents an 80-record average of a simulated LDV signal with $m = 0.001$ radian and an additive noise signal-to-noise ratio of 400. This is the same signal used to produce the conventional co-intensity spectrum of Fig. 6.2. Aside from the obvious difference in principle domain, a comparison of the two figures suggests that the folded method may yield somewhat better coherences in the presence of random noise. Comparisons of conventional and folded co-intensity spectra for a variety of different noise levels support the above observation although a detailed study of processing gain has not been conducted at this point.

Finally, a comparison of the simulated and actual LDV data was performed using the folded co-intensity algorithm. The folding frequency for the actual LDV signal was taken as 50.2 kHz, which fell at the center of the carrier peak. The results, presented in Fig. 6.6, show good agreement between the spectra of the simulated and actual LDV signals, again indicating that the most important features of an LDV signal have been incorporated in the modeled signal. As in the comparisons described above, the folded co-intensity

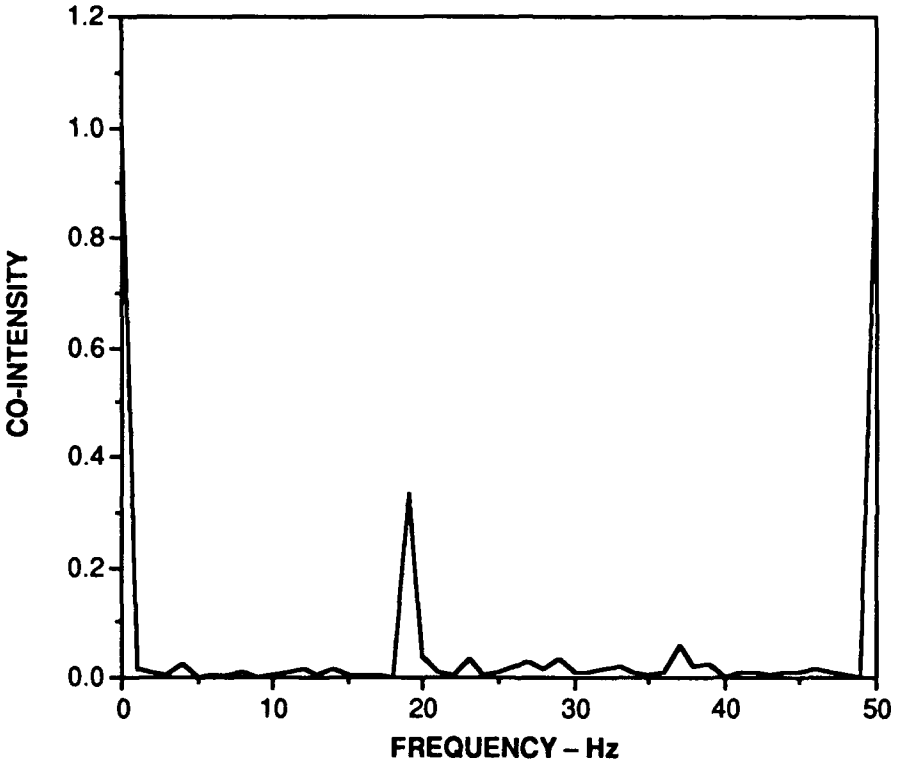

FIGURE 6.5
"FOLDED" CO-INTENSITY SPECTRUM FOR A SIMULATED LDV SIGNAL

The "folded" co-intensity spectrum for a simulated LDV signal with a phase modulation value of 0.001 rad and a signal-to-noise ratio of 400 for the random additive noise term. The spectrum is displayed with one of the two dependent frequencies fixed at a folding frequency of 50 Hz and represents an 80-record coherent average. The frequency scale shown is relative to the folding frequency and the folded Doppler sideband occurs at approximately 20 Hz.

ARL:UT
AS-90-843
MLB - DS
11 - 2 - 90

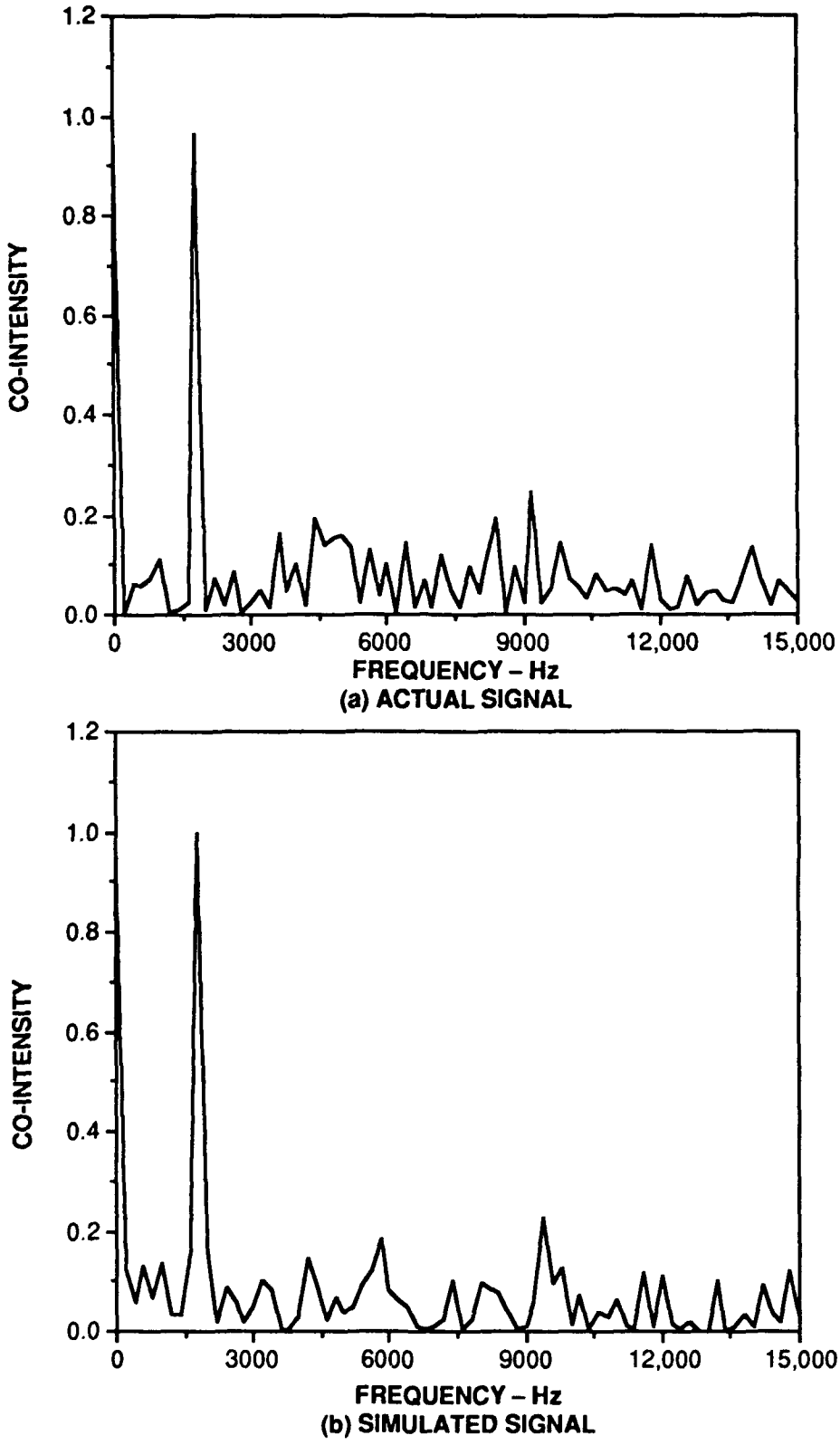

FIGURE 6.6
COMPARISON OF "FOLDED" CO-INTENSITY SPECTRA FROM ACTUAL AND SIMULATED LDV SIGNALS

"Folded" co-intensity spectra for an actual LDV signal (a) and simulated signal (b) with phase modulation values of approximately 0.33 rad. The spectra are displayed with one of the two dependent frequencies fixed at a folding frequency of approximately 50 kHz and represent 16-record coherent averages. The frequency scale shown is relative to the folding frequency and the folded Doppler sideband occurs at approximately 1810 Hz.

ARL:UT
AS-90-844
MLB - DS
11 - 2 - 90

processing of the LDV data appears to produce an improvement in the detected coherence between the carrier and first sideband when compared with the results from the standard co-intensity processing of the signal (Fig. 6.3).

7. SUMMARY AND CONCLUSIONS

In this report a description of our efforts to understand the principles of LDV-based remote acoustic detection, the general characteristics of signals produced by LDV sensors, factors which limit the sensitivity of such systems, and the relative merits of several different processing schemes for LDV acoustic sensors has been presented. The basic single particle forms of LDV signals for two optical arrangements, the differential and reference beam geometries, have been derived and used as the basis for constructing an LDV signal simulation program for use in signal processing studies. The simulated signals consist of a "photon stream" which represents the output from a photon-counting detector. The noise contribution due to the discrete nature of the detection process (shot noise) is simulated using a Poisson distributed random number generator. Additional terms are incorporated in the signal which allow the user to specify the relative contributions of random phase noise and additive random noise to the signal.

In constructing a simulation model for an LDV signal an attempt was made to include the signal properties which are most relevant from a signal processing perspective. Comparisons of results obtained from several different signal processing algorithms using both simulated LDV signals and a sample of actual LDV data suggest that the simulated signals are a reasonable representation of signals which may be obtained from an actual LDV acoustic sensor. The signal simulation program was used extensively in the signal processing studies which followed and provided a great deal of flexibility in specifying the signal characteristics (Doppler signal strength, signal-to-noise ratios, detected photon flux, etc.) for determinations of the merits and limitations of various signal processing schemes.

The initial signal processing study utilized power spectral processing to identify the effects of the model noise sources on the detectability of the Doppler signal. The relationship between the Doppler signal strength and the underlying acoustic field was established and general relationships were determined which related the maximum tolerable noise levels from the various sources to the minimum Doppler signal which could be visually identified in a power spectral plot. Several limitations on Doppler signal detectability were

empirically determined during the course of the study. Lower limits were established for the detected photon flux as a function of Doppler signal strength for a "noiseless" LDV acoustic sensor. The effects of the various model noise sources were then investigated and maximum noise levels as a function of Doppler signal strength were determined. Based on the empirical results of this study, one can conclude that an extension of present demonstrated detection sensitivity by one or two orders of magnitude will require a very "quiet" LDV system if one employs power spectral processing techniques.

Motivated by the relationship between signal detectability and detected photon flux, a set of calculations was then performed to determine the viability of detecting weak acoustic fields in a laboratory demonstration using LDV techniques. The scattered photon flux at a photodetector was determined for two possible LDV configurations constrained to operate in a backscatter geometry. The sensitivity to the various optical parameters of the LDV system was determined. Uncertainties about both the value and applicability of the seawater scattering coefficient used in the calculations raised concerns about the validity of the results. However, based on the inputs used in the calculations, a laboratory demonstration of LDV acoustic sensing appears feasible at sound levels which are one or two orders of magnitude less than those presently detected in laboratory measurements. The uncertainties in the seawater scattering characteristics are being addressed in a separate experimental program which is summarized in the Appendix that follows.

Finally, an initial study was conducted of several potential higher order processing techniques which may provide better discrimination against certain noise sources than can be obtained from power spectral techniques. The methods used in this study employ spectral correlation techniques which highlight fixed phase relationships between various spectral components. The evaluation of bispectral processing schemes for detection of acoustic fields with bispectral signatures (i.e., strong acoustic tones which produce significant higher order Doppler sidebands and acoustic fields which contain bispectral components) has been left for a future study.

An empirical evaluation of the standard spectral correlation function known as the co-intensity was performed and compared with results from power

spectral analysis. The comparisons indicated enhanced processing gain in the presence of random noise sources using co-intensity processing and suggested detection of the Doppler signal may be possible in random noise backgrounds with levels which are approximately twice as large as the maximum tolerable noise levels found in the power spectral processing studies. A more detailed determination of the limitations of this technique remains for a future study. A new algorithm, which utilizes spectral correlation techniques and attempts to exploit symmetries which exist in the LDV spectrum, was developed. Comparisons of results from this "folded co-intensity" with conventional co-intensity results suggest that the folded co-intensity technique may provide enhanced detection coherence for this form of signal.

Future work will include studies of other forms of correlation processing as well as a potential application of bispectral techniques. Quantitative studies will be conducted on potential improved processing schemes to determine the potential processing gains and to establish the limitations of applicability. Finally, it is hoped that data from actual LDV measurements which span a range of Doppler signal strengths and noise levels will become available as an aid both for evaluating various signal processing schemes and for improving our modeled LDV signal.

APPENDIX

SUPPLEMENTARY EXPERIMENTAL PROGRAM

In order to address some of the uncertainties which have arisen during our initial investigations of LDV signal characteristics and the associated signal processing schemes, ARL:UT has begun an experimental program to provide data on several key issues. The experimental equipment to conduct these measurements has been provided through funding from an ARL:UT IR&D contract, except for a vibration isolated optical table which was acquired with ONR funds. To date, participants have included ONR sponsored personnel, an ARL:UT honors scholar, and students from a senior-level engineering laboratory course. At present we are conducting measurements to address two issues (1) the characteristics of the optical noise produced by the illuminating laser and optics train and (2) seawater scattering characteristics. The purpose of this appendix is to provide a brief description of our objectives in these investigations and to discuss the status of the measurements and analysis.

For the optical noise measurements, an attempt is being made to quantify the spectral character and coherence properties of an illuminating laser beam, both at the laser and after passing through various optics elements. As discussions in this report have indicated, tolerable noise levels for Doppler signal detection with small values of the modulation index (corresponding to small acoustic displacements) may be less than the levels of noise found in typical laboratory lasers. It is hoped that by understanding the spectral content and coherence of the optical noise, a method or combination of methods may be found which will reduce the optical noise contributions to an acceptable level. Possible methods might employ active stabilization of the laser, reduced bandwidth data acquisition, and/or signal processing algorithms which will discriminate against various noise components. Optical noise is also introduced as the beam passes through various optical elements. For passive elements such as lenses, mirrors, and beamsplitters found in LDV systems, noise is primarily caused by unwanted motions of the optical elements. The character of noise sources of this type will also be studied to determine their possible effect on LDV measurements and to determine plausible means for minimizing these noise sources.

At present, an initial set of measurements of optical noise from a 10 mW Uniphase HeNe laser and from a long pathlength (several meters) optical arrangement has been completed. The data were acquired using a photodiode

(Hamamatsu S2216-01) and low noise operational amplifier circuit as a photodetector. Intrinsic detector noise was also recorded and typically contributed less than 0.1% to the noise measurements over the bandwidths of interest. The frequency response of the photodetector circuit was also measured using a pulsed light emitting diode and was found to be constant to beyond 50 kHz, which was well beyond the maximum frequency of the measurements (as determined by the setting of a programmable low pass filter). Analysis of the data to determine both the spectral content and the coherence characteristics is under way. The overall noise levels as a function of detector/data acquisition bandwidth will also be calculated.

Future plans include measurements of noise for additional optical arrangements and measurements of noise from a stabilized 1 mW Spectra Physics HeNe laser to compare with the unstabilized laser. The results of these measurements and the implications of the results as they pertain to LDV systems will be documented in a separate report.

A program has also begun to investigate seawater scattering characteristics as they relate to an LDV acoustic sensor. Approximately 20 seawater samples have been obtained from various locations and depths during the RANGEX 1-90 exercise. Using these samples, determination will be made of means and variances for the number of particles passing through the measurement volume per unit time, the resident time of particles, the time between particles, and the particle signal amplitude. Measurements will also be made of the average scattered photon flux at back angles over time periods which are long compared with the average individual particle signal duration. In all the above measurements, scattering volumes comparable to those which might be expected in LDV measurements will be used. Time and resources permitting, the dependences of the scattered photon flux on the scattering angle and the polarization orientation of the illuminating beam will also be investigated.

Presently we have developed and debugged analysis software which will run on a MASSCOMP data acquisition system computer when the data are acquired. An initial configuration for the detector arm has been established and tested using a photomultiplier tube as the photodetector. After a final checkout

of the optics setup and analysis software, data acquisition will commence. Upon completion of the measurements, the ranges of the various parameters discussed above for the different seawater samples will be determined and the impact of these results on an LDV-based remote acoustic sensor will be assessed. The results will also be presented in written documentation.

After completion of these studies, additional experimental investigations of other issues relating to remote sensing using LDV systems might be undertaken. Potential areas of investigation include the optimization of photon counting techniques and/or a data acquisition system for LDV-based acoustic measurements and an investigation of techniques to produce a stable frequency modulated laser beam at low (< 5 kHz) modulation frequencies.

REFERENCES

1. S. Hanish, "Underwater Laser Doppler Hydrophone," in A Treatise on Acoustic Radiation, Vol. 2, Naval Research Laboratory, Washington, D.C., 1983, Chapter 6.

2. J. Jarzynski, D. Lee, J. Vignola, Y. H. Berthelot, and A. D. Pierce, "Fiber Optic Doppler Systems for Remote Sensing of Fluid Flow," Proc. SPIE 925, 250 (1988).

3. P. S. Dubbelday and H. C. Schau, J. Acoust. Soc. Am. 86, 891 (1989).

4. G. D. Hickman, Y. L. Hsu, M. S. Lee, B. S. Bourgeois, S. T. Hsieh, and S. P. Haimbach, "Measurement of Liquid Surface Acoustic Wave Amplitudes using HeNe Laser Homodyne Techniques," Proc. SPIE 925, 263 (1988).

5. M. S. Lee, "The Surface Detection of Underwater Acoustic Signals using a Helium-Neon Laser," M.S. Thesis, Tulane University, 1988 (unpublished).

6. K. J. Taylor, J. Acoust. Soc. Am. 59, 691 (1976); K. J. Taylor, J. Acoust. Soc. Am. 70, 939 (1981).

7. J. P. Sharpe and C. A. Greated, J. Phys. D 20, 418 (1987).

8. E. H. Trinh, M. Gaspar, and H. P. Stevens, NASA JPL Invention Report NPO-17565/7070, National Aeronautics and Space Administration, Jet Propulsion Laboratory, Pasadena, California, September, 1989; NASA Technical Briefs 13, 50 (1989).

9. R. J. Adrian, "Laser Velocimetry," in Fluid Mechanics Measurements, R. J. Goldstein, ed. (Hemisphere Publishing, New York, 1983), pp. 155-244.

10. M. Schwartz, Information Transmission, Modulation, and Noise (McGraw-Hill Book Company, Inc., New York, 1980), pp. 273-274.

11. R. J. Urick, Principles of Underwater Sound for Engineers (McGraw-Hill Book Company, Inc., New York, 1975).

12. Eustace L. Dereniak and Devon G. Crowe, Optical Radiation Detectors (John Wiley and Sons, New York, 1984), pp. 14-18.

13. E. R. Pike, "Photon Correlation Velocimetry," in Photon Correlation Spectroscopy and Velocimetry (Plenum Press, New York, 1976), pp. 246-343.

14. Y. Berthelot, School of Mechanical Engineering, Georgia Institute of Technology, Atlanta, Georgia (private communication); supported by the Office of Naval Research.

15. N. G. Jerlov, Optical Oceanography (Elsevier Publishing Company, New York, 1968), pp. 15-46.

16. S. Q. Duntley, J. Opt. Soc. Am. 53, 214 (1963).

17. O. B. Brown and H. R. Gordon, Appl. Opt. 13, 2874 (1974).

18. R. W. Sheldon, A. Prakash, and W. H. Sutcliffe, Jr., Limnology and Oceanography 17, 327 (1972).

19. A. D. Weidemann, D. M. Lavoie, R. Hollman, and M. R. Wilcox, "Concurrent Particle and Optical Measurements in Western Sargasso Sea", SPIE 925, 113 (1988).

20. L. E. Drain, The Laser Doppler Technique (John Wiley and Sons, New York, 1980).

21. T. Sato and O. Sasaki, Appl. Opt. 17, 3890 (1978).

22. O. Sasaki, T. Sato, and T. Oda, Appl. Opt. 19, 151 (1980).

23. G. Wilson, "Detection and Time Delay Estimation of Non-Gaussian Signals in Noise," Applied Research Laboratories Technical Report No. 90-25 (ARL-TR-90-25), Applied Research Laboratories, The University of Texas at Austin, 1990.

24. R. B. O'Donnell, "Bispectral Investigation of Active Control Processes," M. S. Thesis, The University of Texas at Austin, 1990 (unpublished).

25. W. A. Gardner, Introduction to Random Processes (Macmillan, New York, 1986), pp. 301-309.

26. K. W. Baugh, "Performance Analysis of the Spectral Correlation Intercept Receiver," Applied Research Laboratories Informal Technical Memorandum No. 88-31 (ARL-ITM-88-31), Applied Research Laboratories, The University of Texas at Austin, 1988.

27. H. S. Black, Modulation Theory (D. Van Nostrand Company, Inc., New York, 1953), pp. 184-188.

17 October 1990

DISTRIBUTION LIST FOR
ARL-TR-90-33
TECHNICAL REPORT UNDER CONTRACT N00014-89-J-1967

Copy No.	
	Office of the Chief of Naval Research Department of the Navy Arlington, VA 22217-5000
1	Attn: J. Smith (Code 1211)
	Office of Naval Intelligence Department of the Navy Room 5D675, Pentagon Washington, DC 20350-2000
2	Attn: L. Long (NIC-00R4)
	Office of Naval Technology Department of the Navy Arlington, VA 22217-5000
3	Attn: T. Goldsberry (OCNR23)
	Commander Naval Sea Systems Command Department of the Navy Washington, DC 20362-5101
4	Attn: R. Dosti (06UR)
5 - 16	Commanding Officer and Director Defense Technical Information Center Cameron Station, Building 5 5010 Duke Street Alexandria, VA 22314
	School of Mechanical Engineering Georgia Institute of Technology Atlanta, GA 30332
17	Attn: Yves Berthelot
18	Signal Physics Group, ARL:UT
19	Martin L. Barlett, ARL:UT
20	Thomas G. Muir, ARL:UT
21	Gary R. Wilson, ARL:UT
22	Library, ARL:UT

Distribution List for ARL-TR-90-33 under Contract N00014-89-J-1967
(cont'd)

Copy No.	
23 - 26	Reserve, ARL:UT